nature neuroscience

ARTICLES

https://doi.org/10.1038/s41593-022-01131-4

Check for updates

OPEN

# A CRISPRi/a platform in human iPSC-derived microglia uncovers regulators of disease states

Nina M. Dräger[1], Sydney M. Sattler[1,18], Cindy Tzu-Ling Huang[2,18], Olivia M. Teter[1,3], Kun Leng[1,4,5], Sayed Hadi Hashemi[6], Jason Hong[1], Giovanni Aviles[1], Claire D. Clelland[2,7], Lihong Zhan[2], Joe C. Udeochu[2], Lay Kodama[2,5,8], Andrew B. Singleton[9,10], Mike A. Nalls[9,10,11], Justin Ichida[12,13,14], Michael E. Ward[15], Faraz Faghri[6,9,10,11], Li Gan[2,16] ✉ and Martin Kampmann[1,17] ✉

**Microglia are emerging as key drivers of neurological diseases. However, we lack a systematic understanding of the underlying mechanisms. Here, we present a screening platform to systematically elucidate functional consequences of genetic perturbations in human induced pluripotent stem cell-derived microglia. We developed an efficient 8-day protocol for the generation of microglia-like cells based on the inducible expression of six transcription factors. We established inducible CRISPR interference and activation in this system and conducted three screens targeting the 'druggable genome'. These screens uncovered genes controlling microglia survival, activation and phagocytosis, including neurodegeneration-associated genes. A screen with single-cell RNA sequencing as the readout revealed that these microglia adopt a spectrum of states mirroring those observed in human brains and identified regulators of these states. A disease-associated state characterized by osteopontin (SPP1) expression was selectively depleted by colony-stimulating factor-1 (CSF1R) inhibition. Thus, our platform can systematically uncover regulators of microglial states, enabling their functional characterization and therapeutic targeting.**

Microglia have a central role in brain development and homeostasis as well as in the pathogenesis of many brain disorders[1]. Over the last decade, human genetics have pointed to a central role for microglia in brain diseases such as Alzheimer's disease (AD)[2], where specific disease-associated genetic variants likely act in microglia, redefining them as potential drivers of AD. To understand the molecular mechanisms underlying the role of microglia in disease and to target them therapeutically, it is necessary to bridge the gap between disease-associated genetic variants and changes in microglial function.

A major challenge is that microglia adopt a large number of distinct functional states in health and disease, which are actively being mapped on the molecular level in mice and humans[3–9]. However, we do not systematically understand how these distinct microglial states contribute to brain function and disease, or the molecular mechanisms regulating these states.

A promising approach to tackle these questions is enabled by CRISPR-based functional genomics in differentiated human cell types[10]. Pooled CRISPR interference (CRISPRi) and CRISPR activation (CRISPRa) screens enable scalable modeling of changes in gene expression and genetic screens to uncover regulatory mechanisms. When combined with induced pluripotent stem cell (iPSC) technology, they enable the investigation of cell-type-specific biology in human cells, including those derived from patients[10]. We recently provided a proof of principle for this strategy by establishing CRISPRi and CRISPRa platforms for genetic screens in iPSC-derived neurons[11,12]. However, such screens have not previously been implemented in iPSC-derived microglia due to challenges inherent in available differentiation protocols. Pooled CRISPR screens rely on lentiviral transduction to introduce libraries of single guide RNAs (sgRNAs), but mature microglia are difficult to transduce with lentivirus. This problem could be overcome by introducing sgRNAs at the iPSC stage. However, most existing protocols are lengthy and aim to recapitulate human microglia ontogeny[13–19], resulting in population bottlenecks during differentiation, which can skew the representation of the sgRNA library.

To overcome these challenges, we developed a different approach for the generation of iPSC-derived microglia by generating a human iPSC line inducibly expressing six transcription factors that enable the generation of microglia-like cells in a rapid and efficient 8-day protocol. These induced-transcription factor microglia-like cells (iTF-Microglia) resemble other iPSC-derived microglia[13–19] in their expression profiles, response to inflammatory stimuli, phagocytic capabilities and capacity to be cocultured with iPSC-derived

[1]Institute for Neurodegenerative Diseases, University of California, San Francisco, San Francisco, CA, USA. [2]Gladstone Institute of Neurological Disease, San Francisco, CA, USA. [3]UC Berkeley-UCSF Graduate Program in Bioengineering, University of California, San Francisco, San Francisco, CA, USA. [4]Biomedical Sciences Graduate Program, University of California, San Francisco, San Francisco, CA, USA. [5]Medical Scientist Training Program, University of California, San Francisco, San Francisco, CA, USA. [6]Department of Computer Science, University of Illinois at Urbana-Champaign, Urbana, IL, USA. [7]Department of Neurology, University of California, San Francisco, San Francisco, CA, USA. [8]Neuroscience Graduate Program, University of California, San Francisco, San Francisco, CA, USA. [9]Center for Alzheimer's and Related Dementias, National Institutes of Health, Bethesda, MD, USA. [10]Laboratory of Neurogenetics, National Institute on Aging, National Institutes of Health, Bethesda, MD, USA. [11]Data Tecnica International, LLC, Glen Echo, MD, USA. [12]Department of Stem Cell Biology and Regenerative Medicine, Keck School of Medicine, University of Southern California, Los Angeles, CA, USA. [13]Eli and Edythe Broad CIRM Center for Regenerative Medicine and Stem Cell Research at USC, Los Angeles, CA, USA. [14]Zilkha Neurogenetic Institute, Keck School of Medicine, University of Southern California, Los Angeles, CA, USA. [15]National Institute of Neurological Disorders and Stroke, National Institutes of Health, Bethesda, MD, USA. [16]Helen and Robert Appel Alzheimer's Disease Research Institute, Brain and Mind Research Institute, Weill Cornell Medicine, New York, NY, USA. [17]Department of Biochemistry and Biophysics, University of California, San Francisco, San Francisco, CA, USA. [18]These authors contributed equally: Sydney M. Sattler, Cindy Tzu-Ling Huang. ✉e-mail: lig2033@med.cornell.edu; martin.kampmann@ucsf.edu

neurons. By integrating inducible CRISPRi/a machinery into this cell line, we developed a genetic screening system that enables robust knockdown and overexpression of endogenous genes in human microglia. Using this platform, we conducted pooled CRISPRi and CRISPRa screens for modifiers of survival, phagocytosis and inflammatory activation, which uncovered microglia-specific genes controlling these phenotypes. A screen with single-cell RNA sequencing (scRNA-seq) as the readout revealed that these microglia adopt a spectrum of states mirroring those observed in human brains, and pinpointed regulators of specific states, which can enable the functional characterization and therapeutic targeting of these states.

## Results

**Rapid and scalable production of microglia-like cells.** We set out to create a fast, robust and scalable differentiation protocol to differentiate iPSCs to microglia-like cells for use in CRISPR screens. To this end, we developed a strategy based on direct cell fate conversion by overexpression of transcription factors. Based on transcriptomic and developmental data[20–22], we selected six transcription factors highly expressed in human microglia: Hematopoietic Transcription Factor PU.1, MAF BZIP Transcription Factor B (MAFB), CCAAT Enhancer Binding Protein Alpha (CEBPα), CCAAT Enhancer Binding Protein Beta (CEBPβ), Interferon Regulatory Factor 5 (IRF5) and Interferon Regulatory Factor 8 (IRF8). We engineered an iPSC line with two integrated cassettes for the doxycycline-inducible expression of three transcription factors each in the Citrate Lyase Beta Like (CLYBL) and Adeno-Associated Virus Integration Site 1 (AAVS1) safe-harbor loci (Fig. 1a).

We established a simple three-step protocol to differentiate these iPSCs into microglia-like cells, which we will refer to as iTF-Microglia, in only 8 days (Fig. 1b). After doxycycline induction of transcription factor expression on day 0, medium was supplemented with cytokines granulocyte-macrophage colony-stimulating factor (GM-CSF) and interleukin-34 (IL-34) on day 2 to promote differentiation and survival. On day 4, the medium was additionally supplemented with the cytokines macrophage colony-stimulating factor (M-CSF) and transforming growth factor β (TGF-β). iTF-Microglia reached a fully ramified morphology on day 8 and maintained excellent viability for at least another 8 days (Fig. 1b). We generally have continued doxycycline supplementation beyond day 8; however, this is not necessary for survival (Extended Data Fig. 1a,b). We confirmed robust inducible expression of the transgenic transcription factors (Fig. 1c).

The canonical microglia markers GPR34 and IBA1 were expressed in the iTF-Microglia at day 8 of differentiation (Fig. 1d). RNA sequencing (RNA-seq) confirmed downregulation of iPSC markers and induction of microglia markers in iTF-Microglia at day 9 and day 15 (Fig. 1e and Supplementary Table 1). Some markers, such as *P2RY12*, *CSF1R*, *CYBB* and *CD14*, slightly increased their expression from day 9 to day 15, indicating further incremental maturation from day 9 to day 15. While the transcriptomic signature of our microglia was distinct from primary human microglia, it was comparable to that of several other iPSC-derived microglia protocols (Fig. 1f and Extended Data Fig. 1c).

In conclusion, our results indicate robust expression of microglia markers in iTF-Microglia. Importantly, our differentiation strategy is compatible with large-scale pooled sgRNA screens, whereas classical protocols create population bottlenecks (Extended Data Fig. 1d).

**Functional characterization of iTF-Microglia.** Next, we asked whether iTF-Microglia recapitulated cellular functions of human microglia. iTF-Microglia robustly phagocytosed fluorescent beads (Extended Data Fig. 2a) and rat synaptosomes (Fig. 2a,b and Extended Data Fig. 2b). As expected, phagocytosis could be attenuated by the actin polymerization inhibitor Cytochalasin D, since phagocytosis depends on actin dynamics (Fig. 2a,b and Extended Data Fig. 2c).

To test the inflammatory response of iTF-Microglia to bacterial-derived lipopolysaccharide (LPS), we stimulated them with LPS for 24 h. LPS-stimulated iTF-Microglia were less ramified, and instead displayed the ameboid morphology characteristic of activated microglia (Fig. 2c and Extended Data Fig. 2d). RNA-seq revealed that LPS treatment induced immune response genes such as *C3*, *CXCL10*, *IL32* and *SAA1*, and members of the NF-κB pathway, whereas it decreased expression of *TREM2*; markers of homeostatic microglia, such as *P2RY13*; and members of the TGF-β signaling pathway, such as *SLC40A1* (Fig. 2d and Supplementary Table 2). Transcriptomic changes in response to LPS were substantially overlapping with those observed in iPSC-derived microglia we generated following an alternative, previously published[18] protocol (Extended Data Fig. 2e and Supplementary Table 2).

To examine cytokine secretion of iTF-Microglia, we measured the abundance of 36 cytokines secreted in standard culture conditions or following LPS stimulation. Control buffer-treated iTF-Microglia secreted most cytokines at low levels, but higher levels of CCL2 and CXCL1, suggesting the presence of activated cells under control conditions (Fig. 2e), consistent with previous reports suggesting that even primary microglia become partially activated when cultured[23]. When stimulated with LPS, levels of most secreted cytokines increased, most prominently IL-6 with a 14-fold increase and IL-8 and CXCL10, both increased over fourfold (Fig. 2e).

We were able to coculture iTF-Microglia with iPSC-derived glutamatergic neurons (iNeurons) in medium optimized for survival and functionality of both cell types (Methods). Remarkably, cocultured iTF-Microglia displayed a pronounced ramified morphology (Fig. 2f). In conclusion, we show that iTF-Microglia effectively

**Fig. 1 | Rapid differentiation of iPSCs into microglia-like cells (iTF-Microglia) by transcription factor induction. a**, Strategy for stable integration of six transcription factors in AAVS1 and CLYBL loci by TALEN-mediated integration: The doxycycline-inducible reverse transcriptional activator (rtTA3G) is driven by the constitutive CAG promoter. Human MAFB, CEBPα and IRF8 are driven by the tet response element (TRE3G) in the AAVS1 locus. Human PU.1, CEBPβ and IRF5 are driven by TRE3G in the CLYBL locus. All transcription factors are separated from each other via T2A ribosome skipping sequences. **b**, Overview of the differentiation process for generating iTF-Microglia. Top, timeline with media, cytokines and doxycycline (Dox); bottom, representative phase-contrast images of cells on the indicated days. Scale bar, 100 µm. **c**, Expression of six inducible transcription factors during iTF-Microglia differentiation. Transcript abundance (transcripts per million, TPM) of MAFB, CEBPα, IRF8 cassette and the PU.1, CEBPβ, IRF5 cassette at day 0, day 9 and day 15 of differentiation. Mean ± s.d., $n = 3$ biological replicates, $P$ values from two-tailed Student's $t$-test. **d**, Representative immunofluorescence micrographs of iTF-Microglia on day 8 of differentiation stained for microglia markers GPR34 and IBA1. Nuclei were labeled by Hoechst 33342. Scale bar, 100 µm. **e**, Expression of iPSC and microglia marker genes in iPSCs and derived iTF-Microglia on day 9 and day 15 of differentiation. The heatmap displays normalized and gene-centered TPM counts for selected genes (rows) for three biological replicates of timepoints (columns). iTF-Microglia express microglia homeostatic markers and activation markers, while losing their expression of iPSC markers. Asterisks highlight microglia-selective markers. **f**, Principal component analysis (PCA) on the expression of microglia marker genes of iTF-Microglia, human adult ex vivo microglia[60], fetal and adult microglia[13], human myeloid cells[20], other iPSC-microglia (iMG) / iPSC-microglia-like cells (iMGL)[13,18,61] and iPSCs (this study and ref. [61]). Each dot reflects an independent biological sample. Colors represent the different cell types.

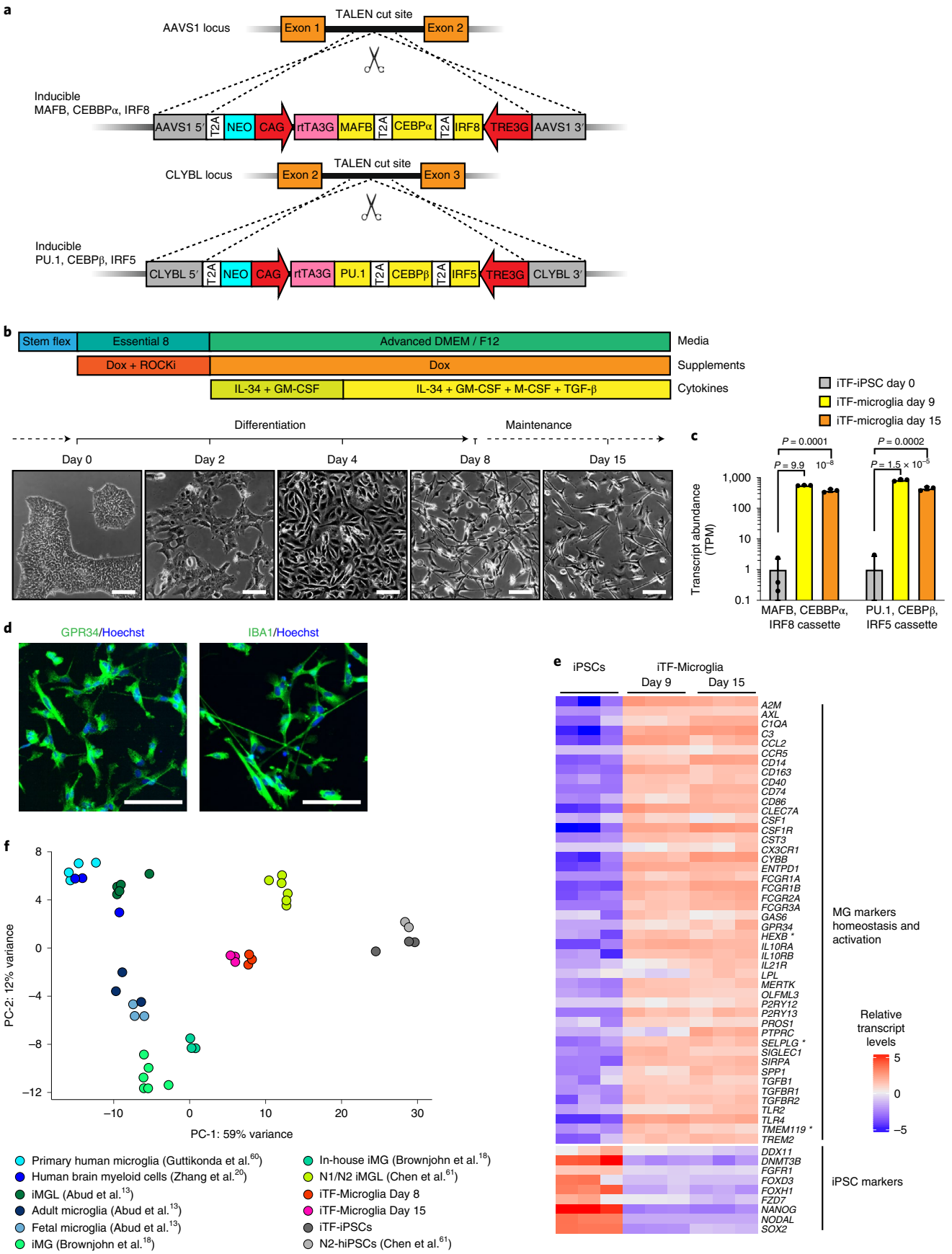
a
AAVS1 locus
TALEN cut site
Exon 1
Exon 2
Inducible
MAFB, CEBBPα, IRF8
AAVS1 5′
T2A
NEO
CAG
rtTA3G
MAFB
CEBPα
IRF8
TRE3G
AAVS1 3′
CLYBL locus
Exon 3
Inducible
PU.1, CEBPβ, IRF5
CLYBL 5′
PU.1
CEBPβ
IRF5
CLYBL 3′
b
Stem flex
Essential 8
Advanced DMEM / F12
Media
Dox + ROCKi
Dox
Supplements
IL-34 + GM-CSF
IL-34 + GM-CSF + M-CSF + TGF-β
Cytokines
Differentiation
Maintenance
Day 0
Day 2
Day 4
Day 8
Day 15
c
iTF-iPSC day 0
iTF-microglia day 9
iTF-microglia day 15
P = 0.0001
P = 9.9
10−8
P = 0.0002
P = 1.5 × 10−5
Transcript abundance (TPM)
1,000
100
10
1
0.1
MAFB, CEBBPα, IRF8 cassette
PU.1, CEBPβ, IRF5 cassette
d
GPR34/Hoechst
IBA1/Hoechst
e
iPSCs
iTF-Microglia
Day 9
Day 15
A2M
AXL
C1QA
C3
CCL2
CCR5
CD14
CD163
CD40
CD74
CD86
CLEC7A
CSF1
CSF1R
CST3
CX3CR1
CYBB
ENTPD1
FCGR1A
FCGR1B
FCGR2A
FCGR3A
GAS6
GPR34
HEXB *
IL10RA
IL10RB
IL21R
LPL
MERTK
OLFML3
P2RY12
P2RY13
PROS1
PTPRC
SELPLG *
SIGLEC1
SIRPA
SPP1
TGFB1
TGFBR1
TGFBR2
TLR2
TLR4
TMEM119 *
TREM2
MG markers homeostasis and activation
Relative transcript levels
5
0
−5
DDX11
DNMT3B
FGFR1
FOXD3
FOXH1
FZD7
NANOG
NODAL
SOX2
iPSC markers
f
PC-2: 12% variance
PC-1: 59% variance
8
4
0
−4
−8
−12
−10
0
10
20
30
Primary human microglia (Guttikonda et al.[60])
Human brain myeloid cells (Zhang et al.[20])
iMGL (Abud et al.[13])
Adult microglia (Abud et al.[13])
Fetal microglia (Abud et al.[13])
iMG (Brownjohn et al.[18])
In-house iMG (Brownjohn et al.[18])
N1/N2 iMGL (Chen et al.[61])
iTF-Microglia Day 8
iTF-Microglia Day 15
iTF-iPSCs
N2-hiPSCs (Chen et al.[61])

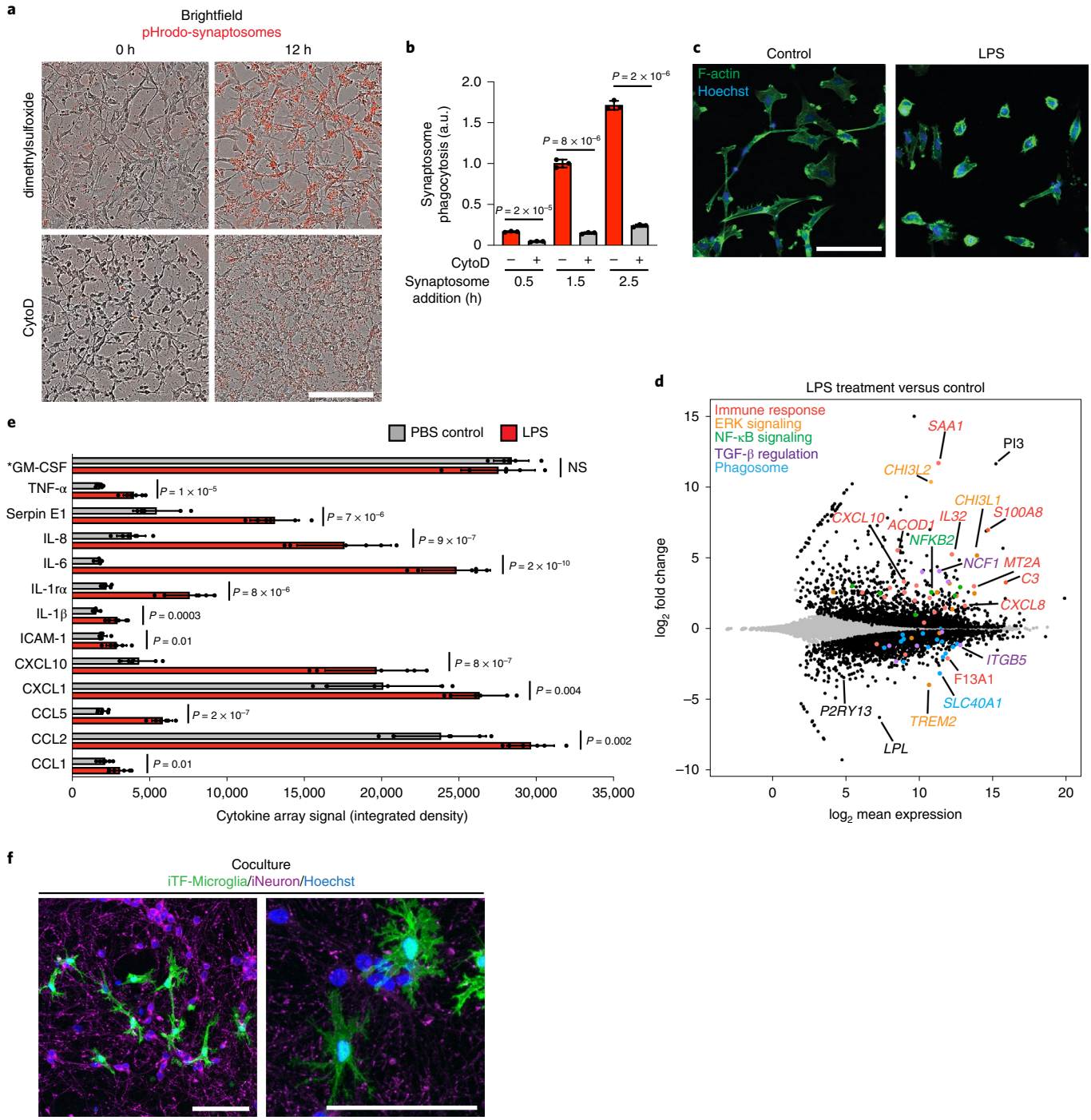


**Fig. 2 | Functional characterization of iTF-Microglia. a**, Phagocytosis of pHrodo-Red-labeled rat brain-derived synaptosomes by iTF-Microglia. Representative images at 0 h and 12 h after synaptosome addition are shown. Treatment with 5 µM actin polymerization inhibitor Cytochalasin D decreases phagocytosis. Scale bar, 100 µm. **b**, Phagocytosis of pHrodo-labeled rat brain-derived synaptosomes with or without Cytochalasin D treatment was quantified by flow cytometry at 0.5 h, 1.5 h and 2.5 h after synaptosome addition (mean ± s.d., $n = 3$ biological replicates; $P$ values from two-tailed Student's $t$-test). **c**, Morphological changes of iTF-Microglia after LPS treatment are visualized by fluorescence microscopy. Samples were treated for 24 h with 100 ng ml$^{-1}$ LPS or buffer control and fixed samples were stained with Alexa Fluor 488-phalloidin for F-actin (green) and with Hoechst 33342 for nuclei (blue). Scale bar, 100 µm. **d**, Transcriptomic changes caused by 50 ng ml$^{-1}$ LPS treatment in day 15 iTF-Microglia ($n = 3$ biological replicates). DEGs ($P_{adj} < 0.05$, two-tailed Student's $t$-test) are labeled in black (increase). Other colors label genes associated with specific pathways that are discussed in the main text. **e**, Cytokines secreted by iTF-Microglia. Analysis of cytokine array signal (integrated density of dot blots) from supernatants of cultures treated with LPS or buffer control (mean ± s.d., $n = 6$ biological replicates; $P$ values from two-tailed Student's $t$-test). *GM-CSF is a component of the culture medium. **f**, Coculture with iPSC-derived excitatory neurons promotes ramified morphology of iTF-Microglia. Representative fluorescence micrographs at low and high magnification of day 9 iTF-Microglia after 24 h in coculture. iTF- Microglia express membrane-localized Lck-mNeonGreen (green). Neurons are stained for the pre-synaptic marker synaptophysin (magenta). Nuclei are stained with Hoechst 33342 (blue). Scale bars, 100 µm. AU, arbitrary units; NS, not significant.

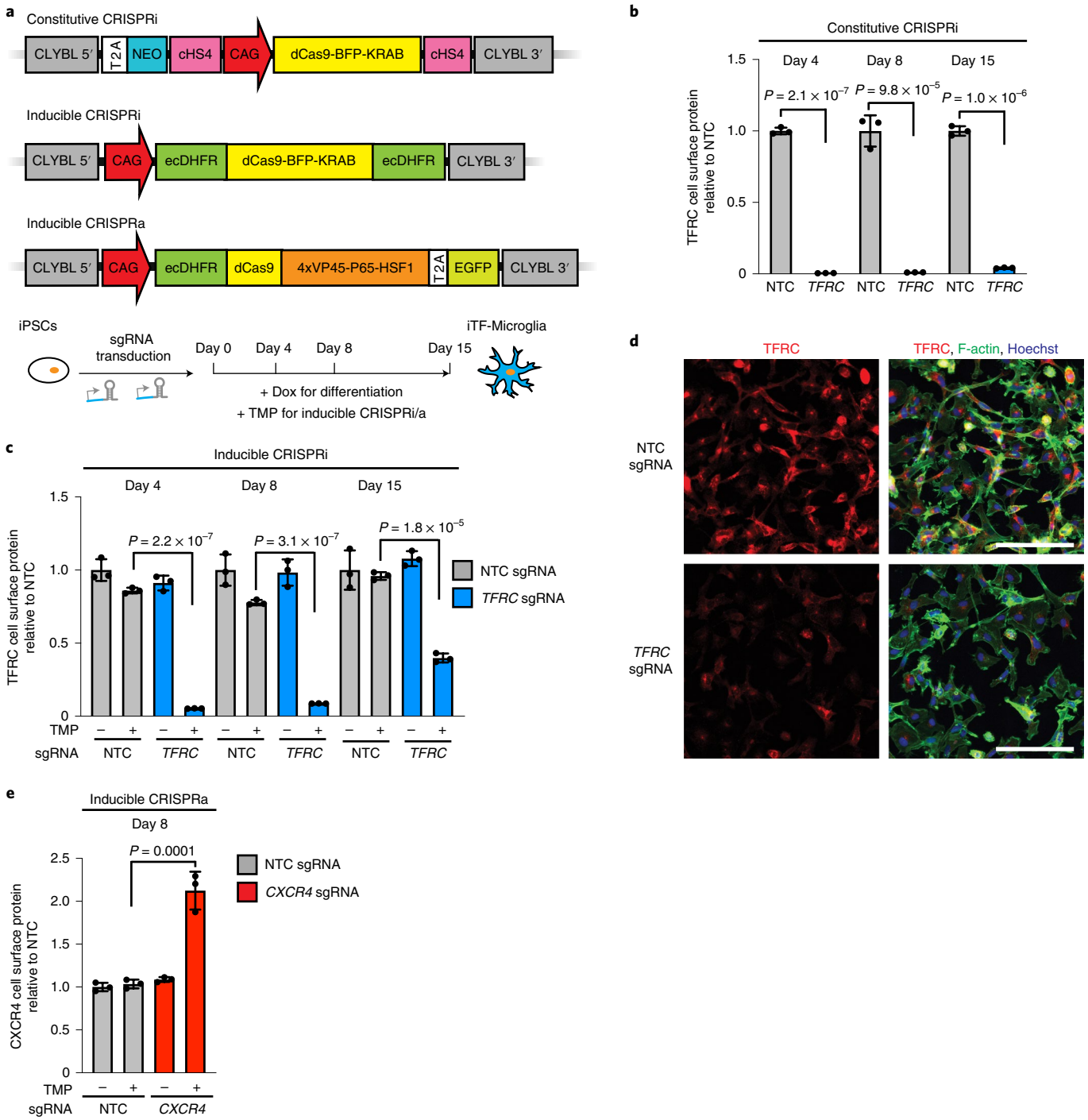


**Fig. 3 | Gene knockdown and overexpression by CRISPRi and CRISPRa in iTF-Microglia. a**, Strategies for constitutive and inducible CRISPRi/CRISPRa in iTF-Microglia. Top, for constitutive CRISPRi, a dCas9-BFP-KRAB construct (catalytically dead Cas9 (dCas9) fused to BFP and the KRAB transcriptional repressor domain) is expressed from the constitutive CAG promotor integrated into the CLYBL safe-harbor locus. Middle, for inducible CRISPRi, dCas9-BFP-KRAB is tagged with ecDHFR degrons. Bottom, for inducible CRISPRa, CAG promotor-driven ecDHFR-dCas9-VPH was stably integrated into the CLYBL locus. VPH, activator domains containing 4× repeats of VP48, P65 and HSF1. Addition of TMP stabilizes the inducible CRISPRi/a machineries. **b**,**c**, Functional validation of constitutive (**b**) or inducible (**c**) CRISPRi activity via flow cytometry of TFRC surface protein level stained iTF-Microglia expressing a TFRC-targeting sgRNA or an NTC sgRNA at different days of differentiation (mean ± s.d., $n = 3$ biological replicates; $P$ values from two-tailed Student's $t$-test). **c**, TMP was added to induce CRISPRi activity where indicated. **d**, Functional validation of inducible CRISPRi activity via TFRC immunofluorescence (IF) microscopy on day 8. Top row, NTC sgRNA. Bottom row, sgRNA targeting *TFRC*. TFRC, red; F-actin, green; nuclei, blue. Scale bar, 100 μm. **e**, Functional validation of inducible CRISPRa activity via flow cytometry of CXCR4 surface protein level staining in iTF-Microglia expressing *CXCR4* sgRNA or NTC sgRNA (mean ± s.d., $n = 3$ biological replicates; $P$ values from two-tailed Student's $t$-test). TMP was added to induce CRISPRa activity where indicated.

phagocytose synaptosomes, respond to LPS and can be cocultured with iPSC-derived neurons.

**Gene perturbation by CRISPRi and CRISPRa in iTF-Microglia.** Next, we established CRISPRi and CRISPRa in iTF-Microglia to enable robust knockdown and overexpression of endogenous genes, as well as large-scale loss- and gain-of-function genetic screens. Following the strategy we previously established in human iPSC-derived neurons[11,12], we stably integrated constitutive CRISPRi machinery, inducible CRISPRi machinery or inducible CRISPRa machinery into safe-harbor loci of iPSCs also engineered with the inducible microglial transcription factors (Fig. 3a). In the constitutive CRISPRi line, the expression cassette contains a CAG promotor-driven dCas9-BFP-KRAB. In the inducible CRISPRi cassette, this CRISPRi machinery is flanked on both the N and the C termini with dihydrofolate reductase (DHFR) degrons. In the absence of the small molecule trimethoprim (TMP), DHFR degrons cause proteasomal degradation of fused proteins. Addition of TMP stabilizes the degron-tagged CRISPRi machinery. The inducible CRISPRa machinery consists of a DHFR-dCas9-VPH construct, which is similarly stabilized in the presence of TMP. Inducible CRISPRi/a systems enable flexible timing of the onset of gene perturbation in cells already expressing sgRNAs. This feature is particularly important for experiments in microglia: it enables lentiviral delivery of sgRNAs to occur in iPSCs, which are much more amenable to lentiviral infection than microglia, without prematurely affecting genes that may be relevant for differentiation. We confirmed a normal karyotype for the resulting monoclonal cell lines (Extended Data Fig. 3).

To validate CRISPRi activity, we transduced iPSCs with a lentiviral construct expressing an sgRNA targeting the transferrin receptor gene (*TFRC*) or a nontargeting control (NTC) sgRNA. In cells expressing the constitutive CRISPRi machinery, knockdown of *TFRC* was robust in iPSCs and iTF-Microglia both on the protein level (Fig. 3b and Extended Data Fig. 4a) and on the messenger RNA level (Extended Data Fig. 4c,e). In cells expressing the inducible CRISPRi machinery, *TFRC* knockdown was completely dependent on the presence of TMP, and effective on the mRNA and protein levels, albeit with reduced knockdown compared with the constitutive CRISPRi system (Fig. 3c,d and Extended Data Fig. 4b,d,f). For additional target genes we tested, we found examples of excellent knockdown (around 80%) with both the constitutive and the inducible systems for *INPP5D* (Extended Data Fig. 4g,h), but also an example of a gene (*PICALM*) that was effectively knocked down by 90% with the constitutive CRISPRi (Extended Data Fig. 4i), but not by inducible CRISPRi (Extended Data Fig. 4j). Despite these limitations of our current inducible CRISPRi system, we decided to use it for the studies presented in this study, since it enabled us to induce CRISPRi knockdown only upon differentiation, rather than in the iPSC state, thus reducing the likelihood of recovering phenotypes due to effects in iPSCs or on differentiation itself.

Next, we validated the functionality of the inducible CRISPRa machinery by testing the induction of the endogenous gene *CXCR4*. We observed a robust and tightly inducible increase of *CXCR4* levels in iPSCs and iTF-Microglia on the mRNA level (Extended Data Fig. 4l,m) and the protein level (Fig. 3e and Extended Data Fig. 4k).

**CRISPRi screen for microglial survival and proliferation.** Our first application of the inducible CRISPRi iTF-Microglia platform was to identify modifiers of microglia survival and proliferation in a pooled genetic screen (Fig. 4a). First, we transduced the iPSCs with our next-generation lentiviral CRISPRi sgRNA library targeting the 'druggable genome'[24]. This library consists of sgRNAs targeting 2,325 genes encoding kinases, phosphatases and other classes of druggable proteins, with five sgRNAs per gene and 500 NTC sgRNAs. After library transduction, iPSCs were differentiated into iTF-Microglia by addition of doxycyline and TMP was added to induce CRISPRi activity. iTF-Microglia were collected before differentiation (day 0) and on day 15 post-induction. Frequencies of cells expressing each sgRNA were determined by next-generation sequencing to uncover genes for which sgRNAs showed significant changes in frequency, indicating a survival or proliferation phenotype (Fig. 4a and Supplementary Table 3).

We compared the results from the iTF-Microglia survival screen with our previously published[11] CRISPRi survival screens in iPSC-derived neurons (Fig. 4b) and iPSCs (Extended Data Fig. 5a). We found that genes affecting microglial survival, neuronal survival and iPSC survival were largely distinct. Knockdown of cholesterol biogenesis enzymes and V-ATPase subunits drastically reduced neuronal but not microglial survival (Fig. 4b). Conversely, knockdown of members of the colony stimulating factor (CSF) receptor family (*CSF1R*, *CSF2RB*, *CSF2RA*) strongly reduced the survival of microglia but not neurons (Fig. 4b) or iPSCs (Extended Data Fig. 5a), consistent with the role of CSF receptors in the development and survival of microglia and macrophages[25–28]. We validated CSF1R essentiality in a time-course experiment (Fig. 4c). The toxicity of CSF1R knockdown became pronounced only in differentiated iTF-Microglia (from day 8 onwards), consistent with the microglia-specific role of CSF1R.

Interestingly, the knockdown of several genes, including *CDK8* and *TGFBR2*, increased abundance of iTF-Microglia in our screen (Fig. 4b). However, we found that *CDK8* and *TGFBR2* knockdown resulted in decreased levels of the microglia marker IBA1 (Extended Data Fig. 5b,c), suggesting disrupted microglial differentiation. Indeed, inhibition of TGF-β signaling has been shown to compensate for loss of *Oct4* pluripotency signaling[29] and microglia have been shown to be absent in TGF-β1-deficient mice[30]. *CDK8* expression has been shown to correlate with stem cell pluripotency[31], and hence loss of *CDK8* expression could cause iPSCs to differentiate into a nonmicroglial state. This disruption of microglial differentiation was not specific to our iTF-Microglia differentiation protocol, since knockdown of *CDK8* also decreased IBA1 levels in iPSC-derived microglia we generated using a non-transcription-factor-based differentiation protocol[18] (Extended Data Fig. 5d,e).

Induction of *CDK8* and *TGFBR2* knockdown on day 8 in fully differentiated iTF-Microglia did not result in proliferation, and in the case of *TGFBR2* knockdown even resulted in a very slight decrease in survival (Extended Data Fig. 5f). By contrast, knockdown of *CSF1R* in day 8 iTF-Microglia reproduced the phenotype observed in the initial screen (Extended Data Fig. 5f).

**CRISPRi screen for modifiers of microglial activation.** In a second screen, we aimed to identify modifiers of inflammatory activation of microglia. For this screen, we chose cell-surface levels of cluster of differentiation 38 (CD38) as a readout for microglial activation. CD38, also known as cyclic ADP ribose hydrolase, is induced by LPS treatment in primary microglia[32] and in our iTF-Microglia (Extended Data Figs. 2e and 5g). CD38 plays several roles in microglial activation, including in the secretion of proinflammatory cytokines[33] and in activation-mediated cell death[32]. Altogether, these data suggest that CD38 is both a marker and an important effector for the activation of microglia and is therefore a suitable marker for a screen for inflammation modifiers.

The screen for modifiers of microglial activation was conducted as shown in Fig. 4d. Briefly, iPSCs expressing the inducible CRISPRi machinery were transduced with the pooled sgRNA library described above. The cells were then differentiated into iTF-Microglia, stained for cell-surface CD38 using a fluorescently tagged antibody and subjected to fluorescence-activated cell sorting (FACS) into $CD38^{low}$ and $CD38^{high}$ populations. Frequencies of cells expressing each sgRNA were quantified in these populations using next-generation sequencing.

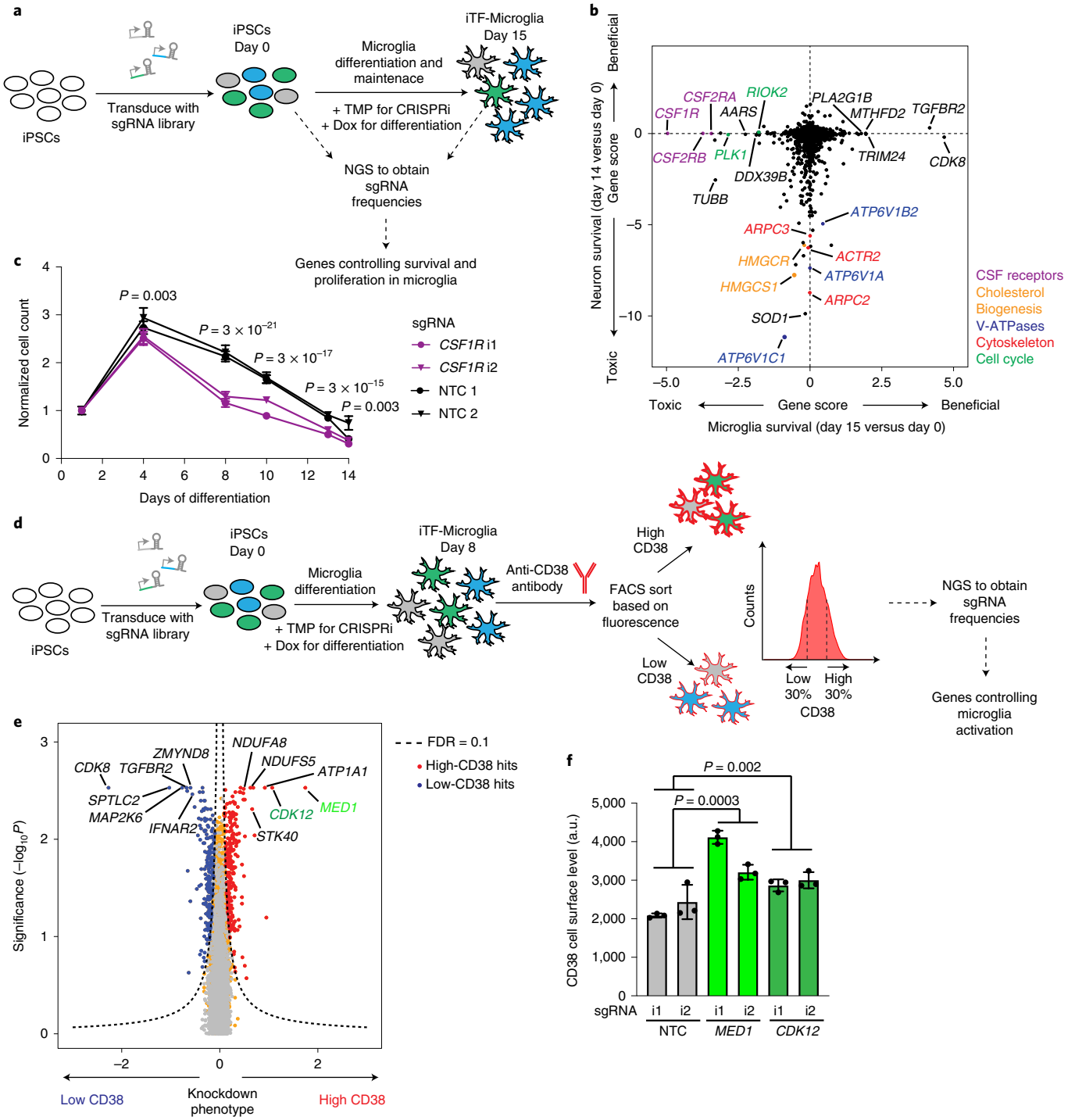


**Fig. 4 | Identification of modifiers of survival and inflammation by CRISPRi screens. a**, Strategy. **b**, Comparison of Gene Scores from CRISPRi survival screens in iTF-Microglia (this study) versus iPSC-derived neurons[11]. Each dot represents a gene; genes are color-coded by pathways. **c**, Validation of the phenotype of CSF1R knockdown. iTF-Microglia transduced with *CSF1R*-targeting or NTC sgRNAs were imaged on different days after differentiation, and live cells were quantified based on staining with Hoechst 33342. Data are shown as mean ± s.d., $n = 3$ wells per group; 7 fields were imaged for each well; *P* values from two-tailed Student's *t*-test. **d**, Strategy for a CRISPRi screen to identify modifiers of the expression of CD38, a marker of reactive microglia. iPSCs expressing the inducible CRISPRi construct were transduced with the druggable genome sgRNA library. On day 0, doxycyline and cytokines were added to induce microglial differentiation, and TMP was added to induce CRISPRi activity. On day 8, iTF-Microglia were stained for cell-surface levels of CD38 and sorted by FACS into populations with low (bottom 30%) and high (top 30%) CD38 levels. Frequencies of iTF-Microglia expressing a given sgRNA were determined in each population by next-generation sequencing (NGS). **e**, Volcano plot indicating knockdown phenotype and statistical significance (two-sided Mann–Whitney *U*-test) for genes targeted in the CD38 level screen. Dashed line indicates the cut-off for hit genes (false discovery rate (FDR) = 0.1). Hit genes are shown in blue (knockdown decreases CD38 level) or red (knockdown increases CD38 level), nonhit genes are shown in orange and 'quasi-genes' generated from random samples of NTC sgRNAs are shown in gray. Hits of interest are labeled. **f**, Validation of the phenotype of *MED1* and *CDK12* knockdown. CD38 cell-surface levels measured by flow cytometry of day 8 iTF-Microglia targeting *MED1*, *CDK12* compared with NTC sgRNA. Means ± s.d., $n = 3$ biological replicates; *P* values from two-tailed Student's *t*-test. i1, i2 refer to independent CRISPRi sgRNAs targeting the indicated genes.

This CRISPRi screen identified several genes regulating cell-surface levels of CD38 (Supplementary Table 3). Knockdown of two transcriptional regulators, *CDK12* and *MED1*, significantly increased CD38 surface levels in the screen (Fig. 4e) and in validation experiments (Fig. 4f). CDK12 is known to be involved not only in cell cycle progression but also in TNF[34] and noncanonical NF-κB[35] signaling. While these previous reports may suggest a proinflammatory role of CDK12, our findings suggest that the role of CDK12 may be more nuanced or context-dependent, and we designated it for further investigation (see below). Another class of hits whose knockdown increased CD38 levels were members of the mitochondrial Complex I (NADH:ubiquinone oxidoreductase), NDUFA8 and NDUFS5 (Fig. 4e). Knockdown of components of this complex have previously been shown to promote an inflammatory state in macrophages[36], validating our findings.

Taken together, our large-scale CRISPRi screens in iTF-Microglia uncovered microglia-specific survival modifiers and modulators of inflammatory activation, demonstrating the ability of the iTF-Microglia screening platform to identify microglia-specific biology.

**Modifiers of synaptosome phagocytosis by microglia.** Microglial phagocytosis is central to brain homeostasis from development through aging[37]. Dysfunctional or dysregulated phagocytosis has been implicated in neurodegenerative and psychiatric diseases[38–41]. To uncover regulators of microglial phagocytosis, we conducted parallel CRISPRi and CRISPRa screens in iTF-Microglia transduced with sgRNA libraries targeting the 'druggable genome'. After 1.5 h of incubation with pHrodo-Red-labeled synaptosomes isolated from rat brains, iTF-Microglia were sorted via FACS based on the pHrodo-Red fluorescence signal (Fig. 5a), and screens were analyzed as described for the CD38 FACS-based screen.

There was little overlap between CRISPRi and CRISPRa hits (Extended Data Fig. 6a and Supplementary Table 3), confirming our previous findings from screens in diverse biological contexts that overexpression and knockdown screens can provide complementary insights[12,42,43]. A prominent exception was the actin-binding protein *PFN1*, coding mutations in which cause amyotrophic lateral sclerosis (ALS)[44]. *PFN1* had opposing phenotypes on synaptosome phagocytosis upon CRISPRi repression and CRISPRa induction (Fig. 5b). Unexpectedly, knockdown of *CSF1R* increased phagocytosis (Fig. 5b), even though, as we had previously found (Fig. 4b), its knockdown decreased iTF-Microglia survival. Another remarkable hit was the AD risk factor *INPP5D*, knockdown of which slightly increased phagocytosis. Overexpression of *CD209*, a C-type lectin receptor present on the surface of macrophages and dendritic cells, greatly increased synaptosome phagocytosis (Fig. 5b). We validated these phenotypes from the primary CRISPRi screen individually in iTF-Microglia (Extended Data Fig. 6b) and in iPSC-derived microglia generated an alternative protocol[18] (Extended Data Fig. 6c).

We further investigated the CRISPRa hits *PFN1* and *CD209*. We validated upregulation of both genes by quantitative PCR (qPCR) (Extended Data Fig. 6e). Pattern-recognition receptor CD209 has previously been shown to regulate phagocytic capacity in macrophages[45]. To investigate substrate specificity of CD209, we monitored phagocytosis of two different substrates, pHrodo-Red-labeled synaptosomes and yellow-green (YG)-fluorescently labeled beads, either alone or in combination (Fig. 5c). Overexpression of CD209 increased phagocytosis of synaptosomes, but had a much smaller effect on bead phagocytosis (Fig. 5c), suggesting substrate specificity. However, when challenging iTF-Microglia with a mixture of beads and synaptosomes, bead phagocytosis was robustly increased, suggesting that synaptosomes might stimulate general phagocytosis via CD209.

*PFN1* overexpression increased levels of F-actin in iTF-Microglia (Fig. 5d), consistent with previous finding that moderate overexpression of PFN1 induces long stress fiber-like actin cables[46]. This process could disturb orchestrated actin polymerization at the membrane and thus decrease phagocytosis. In addition to direct effects on the actin cytoskeleton, *PFN1* knockdown has also been reported to result in anti-inflammatory changes[47]. Indeed, we observed transcriptional changes in immune-related genes and AD risk genes upon *PFN1* overexpression in iTF-Microglia (Fig. 5e and Supplementary Table 4).

In conclusion, our complementary CRISPRi and CRISPRa screens identified known as well as novel phagocytosis modulators in microglia, which were validated in iPSC-derived microglia generated using an alternative protocol.

**Distinct transcriptional states of iTF-Microglia.** Several genes had CRISPRi phenotypes in more than one of the large-scale screens that we conducted (Extended Data Fig. 6f and Supplementary Table 3). We therefore hypothesized that some hit genes were not dedicated factors required for specific microglial processes, but rather regulators of distinct functional states. To test this hypothesis and gain more detailed insights into the mechanisms by which genes affect microglial functions, we selected 39 hit genes of interest, most of which had phenotypes in more than one of the large-scale primary screens (Extended Data Fig. 6f and Supplementary Table 3), for characterization in a CRISPR droplet sequencing (CROP-seq) screen, which couples CRISPRi perturbation to scRNA-seq. We introduced an sgRNA library targeting these genes (Supplementary Table 5) into iPSCs, induced iTF-Microglia differentiation and CRISPRi activity, and performed scRNA-seq of 58,302 iTF-Microglia on day 8 (Fig. 6a and Supplementary Table 6).

Unsupervised clustering and Uniform Manifold Approximation and Projection (UMAP) dimensional reduction of the single-cell transcriptomes uncovered distinct clusters (Fig. 6b). In one cluster, a high proportion of transcripts mapped to mitochondrial transcripts, suggesting damaged or dying cells; this cluster was

**Fig. 5 | Identification of modifiers of phagocytosis by CRISPRi and CRISPRa screens. a**, Strategy for modifier screen based on the uptake of pHrodo-labeled rat synaptosomes. **b**, Volcano plots summarizing knockdown and overexpression phenotypes and statistical significance (two-sided Mann–Whitney *U*-test) for genes targeted in the pooled phagocytosis screens. Left, CRISPRi screen; right, CRISPRa screen. Dashed lines, Gene Score cut-off for hit genes (FDR = 0.1). Hit genes are shown in blue (knockdown decreases phagocytosis) or red (knockdown increases phagocytosis), nonhit genes are shown in orange and 'quasi-genes' generated from random samples of NTC sgRNAs are shown in gray. Hits of interest are labeled. **c**, Competitive phagocytosis assay to test substrate specificity of *CD209* overexpression. Flow cytometry measurement of phagocytosis of pHrodo-Red-labeled synaptosomes (left, either synaptosomes alone or together with beads) and green, fluorescent beads (right, either beads alone or together with synaptosomes) by iTF-Microglia expressing either NTC sgRNAs or sgRNAs targeting *CD209*. Values represent mean ± s.d. of $n = 3$ biological replicates. Data were analyzed using two-tailed Student's *t*-test. **d**, Representative fluorescent images demonstrating higher F-actin staining in CRISPRa iTF-Microglia at day 8 with *PFN1* sgRNAs compared with NTC sgRNAs (left). Scale bar, 50 µm. Right, integrated F-actin intensity per cell of CRISPRa iTF-Microglia at day 8 with *PFN1* sgRNAs or NTC sgRNAs. Mean ± s.d., $n = 5$ fields of view from 3 different wells per sgRNA. *P* values from two-tailed Student's *t*-test. **e**, Transcriptomic changes caused by *PFN1* overexpression in day 8 iTF-Microglia ($n = 3$ biological replicates). DEGs ($P_{adj} < 0.05$, two-tailed Student's *t*-test) are labeled in black. Other colors label genes associated with specific pathways that are discussed in the main text. *AD risk genes. a1, a2 refer to independent CRISPRa sgRNAs targeting the indicated genes.

removed from downstream analysis (Extended Data Fig. 7a). Two clusters exclusively contained cells expressing sgRNAs targeting *CDK8* or *TGFBR2* (Fig. 6b and Extended Data Fig. 7b). These cells expressed high levels of the pluripotency marker *SOX2*, but low levels of the microglia marker *CSF1R* (Extended Data Fig. 7c). Together with our previous experiments showing reduced IBA1 levels for iTF-Microglia targeting *CDK8* and *TGFBR2* (Extended Data Fig. 5b,c), these findings suggested disrupted microglial

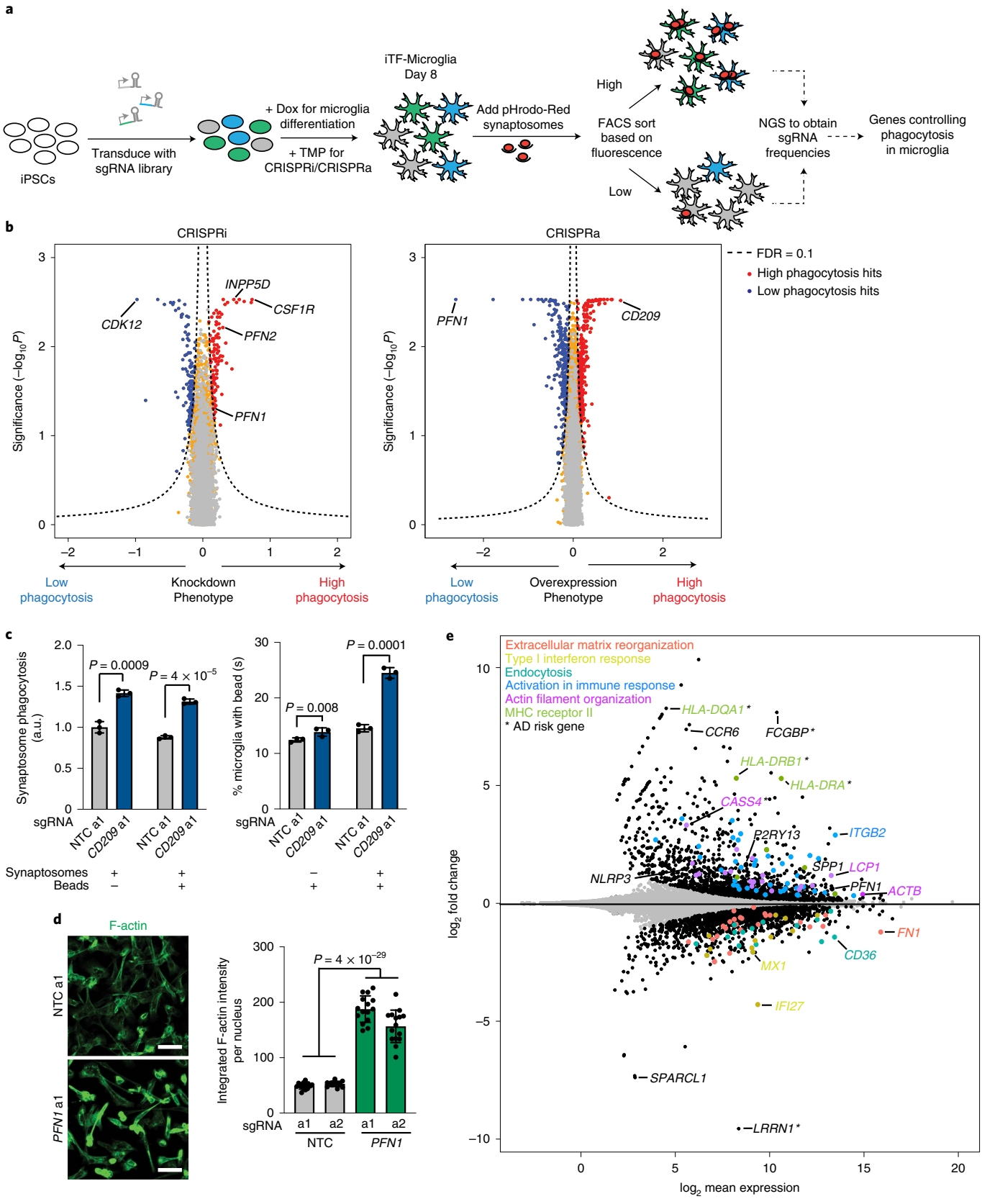

differentiation. We removed those clusters from further analysis and retained the remaining cluster, which was characterized by high levels of *CSF1R* expression (Extended Data Fig. 7c). Importantly, 92.4% of cells expressing NTC sgRNAs were part of the cluster with high levels of *CSF1R* expression, confirming the high efficiency of our microglial differentiation protocol for unperturbed cells.

Unsupervised clustering and UMAP dimensional reduction of the remaining 19,834 iTF-Microglia revealed nine transcriptionally distinct clusters (Fig. 6c and Extended Data Fig. 7d). Microglia heterogeneity in response to different environmental conditions in the brain has been extensively studied[48], but we were surprised to observe a wealth of distinct transcriptional states in the cultured iTF-Microglia. Importantly, NTC sgRNAs are represented in cells in every cluster (Extended Data Fig. 7d), suggesting the observed heterogeneity is an innate quality of the iTF-Microglia.

Principal component analysis identified two major biological axes broadly defining these states. The first principal component (PC1) corresponded to a polarized axis of inflammatory activation: starting from a central homeostatic state (cluster 6), one direction was defined by interferon-induced gene expression, whereas the other direction was defined by induction of chemokines (Fig. 6d and Extended Data Fig. 7e). The second principal component (PC2) captured markers of proliferation, mainly in cluster 7 (Fig. 6e and Extended Data Fig. 7f).

To further interpret each transcriptional microglial state, we performed differential gene expression analysis across the clusters (Supplementary Table 7) and named each cluster according to characteristic transcriptomic signatures (Fig. 6f).

Clusters 1 and 2 are both defined by high expression of interferon-induced genes and the complement gene *C3*. Cluster 1 is uniquely defined by high expression of chemokine *CXCL10*. Subsets of microglia characterized by upregulation of interferon response genes have been described in mouse models of neurodegeneration[4].

Cluster 3 is defined by the high expression of *SPP1* (Fig. 6g), which encodes osteopontin[49]. Importantly, *SPP1* is upregulated in several disease-associated microglial states, including disease-associated microglia[5] and activated response microglia[50] in AD mouse models, and late-response microglia in CK-p25 mouse models of neurodegeneration[4]. SPP1-positive microglial states are also enriched in patients with multiple sclerosis and mouse models[8] and enriched in microglia in the aging human brain[9]. Furthermore, *SPP1* is highly expressed in glioma-associated microglia in mice and humans, where high expression of *SPP1* is associated with poor prognosis[51]. Using flow cytometry, we found that SPP1-positive microglia have a slightly increased phagocytic activity, whereas CCL13-positive microglia have substantially decreased phagocytic activity (Fig. 6h). Integration of our iTF-Microglia dataset with a recent scRNA-seq dataset containing 16,242 human microglia from control and AD patient brains[3] showed conservation of the SPP1-positive microglial state (Fig. 6i). The proportion of SPP1-positive microglia was substantially increased in patients with AD compared with controls (Fig. 6j). Notably, it remains to be determined how the SPP1$^+$ microglial state affects the pathogenesis of different diseases, since SPP1 has been linked to both proinflammatory and anti-inflammatory responses[49]. This question has been challenging to address since we have lacked tools to manipulate the SPP1$^+$ state of microglia.

Cluster 4 is defined by expression of pro-apoptotic p53 signaling genes, and cluster 5 by expression of metallothionines. Cluster 6 is defined by the absence of interferon response genes or chemokines, and thus we interpreted it as representing more homeostatic microglia. Cluster 7 is characterized by the expression of proliferation markers such as *TOP2A* and *MKI67*. Clusters 8 and 9 are characterized by the expression of high levels of chemokines such as *CCL2* and *CCL3*. Cluster 9 is uniquely defined by high expression of *CCL13* (Fig. 6g). Such chemokine signatures have recently been found to be a hallmark of human microglia not observed in mice[52].

Taken together, scRNA-seq revealed that many important features of microglia diversity observed in human brains and in disease states are recapitulated in our iTF-Microglia in vitro model.

**CROP-seq uncovers regulators of microglial cell states.** We next identified the differentially expressed genes (DEGs) caused by CRISPRi knockdown of each gene targeted in the CROP-seq screen (Extended Data Fig. 8 and Supplementary Table 8). As expected, knockdown of functionally related genes resulted in shared DEG signatures. For example, knockdown of *CSF1R*, *CSF2RA* and *CSF2RB* resulted in an upregulation of genes encoding the major histocompatibility complex as well as *CD36*, *CD74* and *CD68* (Extended Data Fig. 8 and Supplementary Table 8), which are markers of phagocytic microglia and could explain the increased phagocytic capacity we observed in response to *CSF1R* knockdown (Fig. 5b and Extended Data Fig. 6b).

Given the surprising heterogeneity of iTF-Microglia, we investigated if CRISPRi knockdown of specific genes could control microglial cell states. Indeed, cells containing sgRNAs targeting genes such as *CSF1R*, *CDK12* and *MAPK14* were enriched or depleted from specific clusters (Fig. 7a), and more generally, knockdown of many genes specifically affected the frequency of cell states (Fig. 7b, Extended Data Fig. 9a and Supplementary Table 9).

Knockdown of *CDK12* shifted cells into cluster 9 (CCL13$^+$, chemokine) (Fig. 7a–c). To validate this phenotype, we used a flow cytometry approach in which secretion of CCL13 was inhibited with the transport inhibitor GolgiPlug. CCL13 levels were increased over twofold with knockdown of *CDK12* (Fig. 7d), confirming our screen results. Next, we asked if the shift into cluster 9 might also have functional consequences for the iTF-Microglia. We measured

**Fig. 6 | scRNA-seq reveals distinct and disease-related microglia subclusters. a**, Strategy for the CROP-seq screen. IPSCs expressing inducible CRISPRi machinery were transduced with a pooled library of 81 sgRNAs and CROP-seq vector pMK1334. iPSCs are differentiated to iTF-Microglia and subjected to scRNA-seq to obtain single-cell transcriptomes and to identify expressed sgRNAs. **b**, UMAP of the 28,905 cells in the post-quality control CROP-seq dataset. Cells are colored by sgRNA (*CDK8*, red; *TGFBR2*, orange) and cells with a high percentage of mitochondrial transcripts (blue). Microglia are labeled in green. Each dot represents a cell. **c**, UMAP depicting the 9 different clusters within the 19,834 microglia. Each dot represents a cell. The cells are color-coded based on their cluster membership. **d**,**e**, Ridge plots depicting iTF-Microglia clusters along PC1 (**d**) and PC2 (**e**). PC1 spans inflammation status (interferon activated–homeostatic–chemokine activated) while PC2 spans proliferation status. **f**, Heatmap of iTF-Microglia clusters 1–9 and the relative expression of the top three DEGs (based on $\log_2$ fold differences in expression) of each cluster. **g**, UMAP of distinct marker expression of *CCL13* (left) and *SPP1* (right). *CCL13* is a marker for cluster 9 and *SPP1* is a marker for cluster 3. Cells are colored by the expression levels of the indicated gene. **h**, Phagocytic activity of iTF-Microglia in different states. Flow cytometry measurement of phagocytosis of pHrodo-Red-labeled synaptosomes (left, phagocytosis in CCL13$^{high}$ and CCL13$^{low}$ iTF-Microglia; right, phagocytosis in SPP1$^{high}$ and SPP1$^{low}$ iTF-Microglia). Values represent mean ± s.d. of $n = 3$ biological replicates; *P* values from two-tailed Student's *t*-test. **i**, Integration of single-cell transcriptomes of iTF-Microglia and microglia from post-mortem human brains[3]. In the integrated UMAP, iTF-Microglia (left) with high *SPP1* expression and human brain-derived microglia with high *SPP1* expression (right) form a cluster (dashed outline). **j**, In brains from patients with AD, a higher fraction of microglia is in the SPP1$^{high}$ cluster compared with control brains (data from Olah et al.[3]; *P* value from two-sided Fisher's exact test).

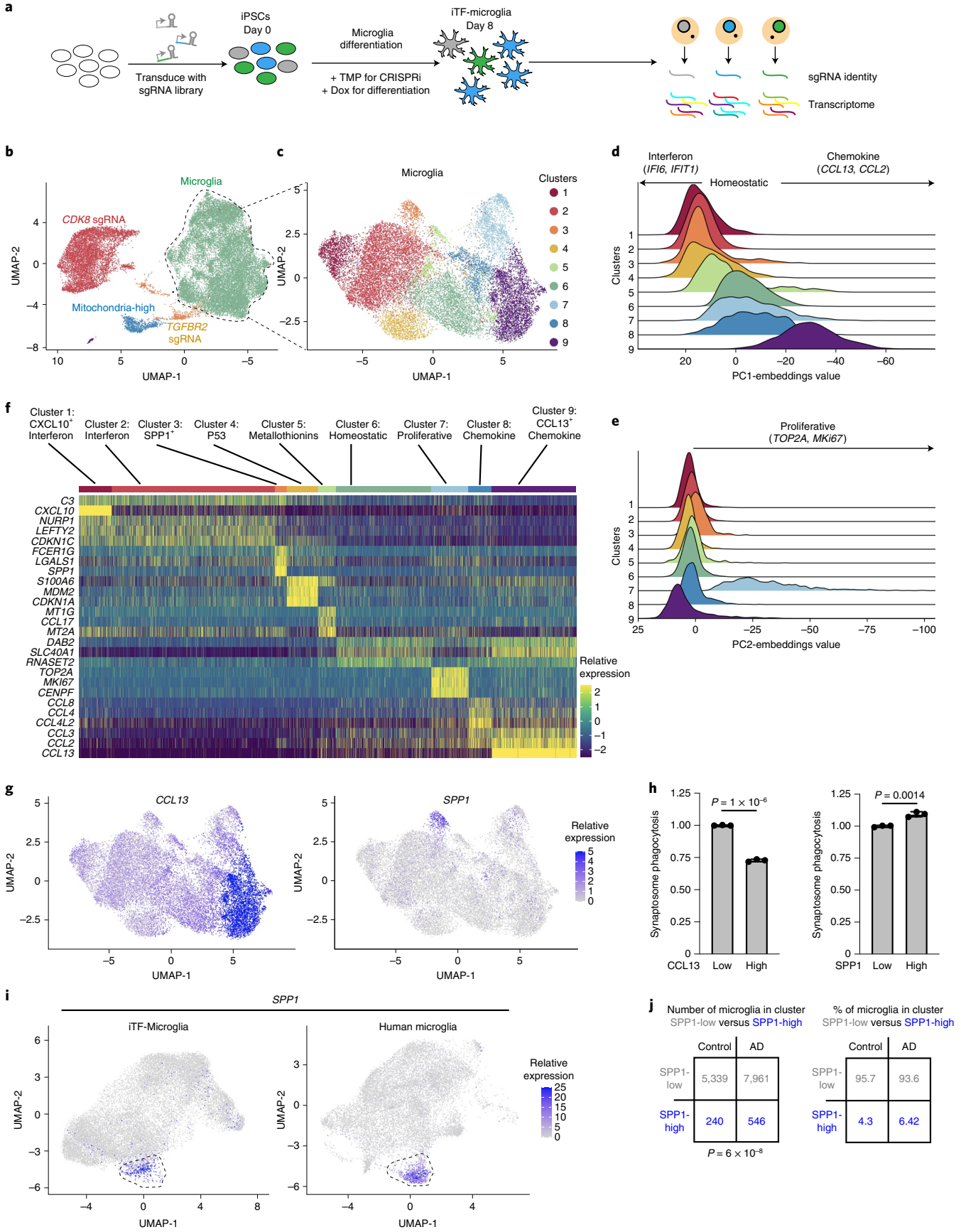
a
iPSCs
Day 0
Transduce with
sgRNA library
Microglia
differentiation
+ TMP for CRISPRi
+ Dox for differentiation
iTF-microglia
Day 8
sgRNA identity
Transcriptome
b
Microglia
CDK8 sgRNA
Mitochondria-high
TGFBR2
sgRNA
UMAP-1
UMAP-2
c
Microglia
Clusters
1
2
3
4
5
6
7
8
9
UMAP-1
UMAP-2
d
Interferon
(IFI6, IFIT1)
Homeostatic
Chemokine
(CCL13, CCL2)
Clusters
PC1-embeddings value
e
Proliferative
(TOP2A, MKi67)
Clusters
PC2-embeddings value
f
Cluster 1:
CXCL10+
Interferon
Cluster 2:
Interferon
Cluster 3:
SPP1+
Cluster 4:
P53
Cluster 5:
Metallothionins
Cluster 6:
Homeostatic
Cluster 7:
Proliferative
Cluster 8:
Chemokine
Cluster 9:
CCL13+
Chemokine
C3
CXCL10
NURP1
LEFTY2
CDKN1C
FCER1G
LGALS1
SPP1
S100A6
MDM2
CDKN1A
MT1G
CCL17
MT2A
DAB2
SLC40A1
RNASET2
TOP2A
MKI67
CENPF
CCL8
CCL4
CCL4L2
CCL3
CCL2
CCL13
Relative
expression
g
CCL13
SPP1
Relative
expression
UMAP-1
UMAP-2
h
P = 1 × 10−6
Synaptosome phagocytosis
CCL13 Low High
P = 0.0014
SPP1 Low High
i
SPP1
iTF-Microglia
Human microglia
Relative
expression
UMAP-1
UMAP-2
j
Number of microglia in cluster
SPP1-low versus SPP1-high
Control AD
SPP1-low 5,339 7,961
SPP1-high 240 546
P = 6 × 10−8
% of microglia in cluster
SPP1-low versus SPP1-high
Control AD
SPP1-low 95.7 93.6
SPP1-high 4.3 6.42

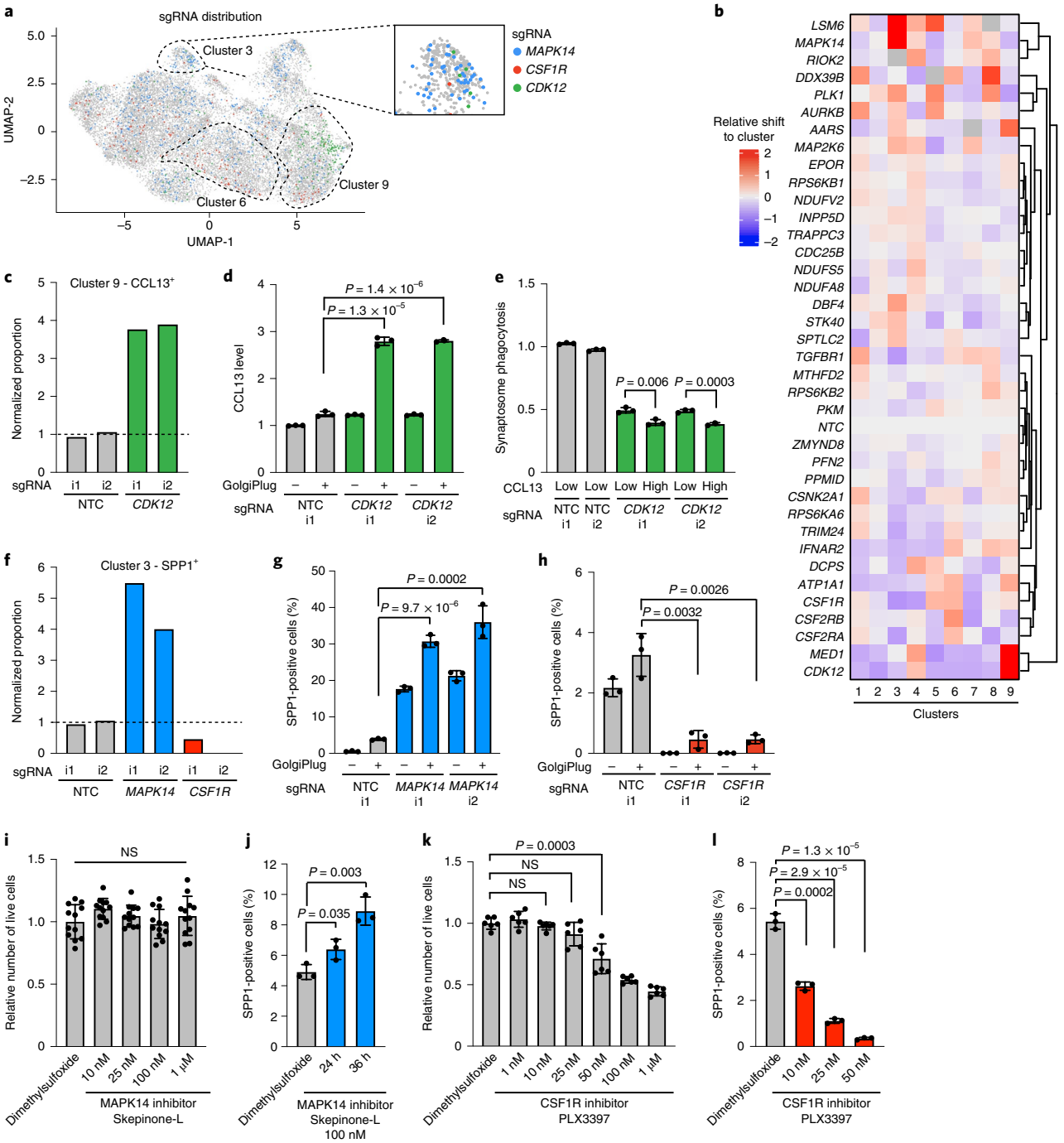


**Fig. 7 | CROP-seq reveals changes in cluster occupancy induced by gene knockdown. a**, UMAP depicts cells with sgRNAs targeting *MAPK14* (blue), *CSF1R* (red) and *CDK12* (green), which are enriched in clusters 3, 6 and 9, respectively. Insert shows cluster 3. **b**, Changes in cluster distribution after CRISPRi knockdown of targeted genes in iTF-Microglia. Heatmap with hierarchical clustering of 37 target genes and NTC and their distribution in clusters 1–9. **c**, Proportion of cells in cluster 9 (CCL13$^+$) expressing either sgRNAs targeting *CDK12* or NTC. **d**, Validation of increased CCL13 in iTF-Microglia expressing sgRNAs targeting *CDK12* compared with NTC. CCL13 levels were measured via flow cytometry ±5 h of GolgiPlug treatment. **e**, Decreased synaptosome phagocytosis of iTF-Microglia expressing sgRNAs targeting *CDK12* compared with NTC. Phagocytosis is further reduced in the CCL13-high population of cells expressing sgRNAs targeting *CDK12*. Phagocytosis was measured via flow cytometry with additional staining for CCL13. **f**, Proportion of cells in cluster 3 (SPP1$^+$) expressing either sgRNAs targeting *MAPK14* or *CSF1R*, or NTC. **g**,**h**, Functional validation of altered percentage of SPP1$^+$ cells in iTF-Microglia expressing sgRNAs targeting *MAPK14* (**g**) or *CSF1R* (**h**) compared with NTC. SPP1 was measured via flow cytometry after treating cells for 5 h with GolgiPlug. **i**, Survival of iTF-Microglia after 24-h treatment with various concentrations of MAPK14 inhibitor Skepinone-L quantified by CellTiter-Glo assay. Mean ± s.d. of $n = 12$ biological replicates, analyzed by one-way analysis of variance (ANOVA). **j**, Percentage of SPP1-positive cells after 100 nM Skepinone-L treatment for 24 h or 36 h. SPP1 was measured via flow cytometry after an additional 5 h of GolgiPlug treatment. **k**, Survival of iTF-Microglia after 24-h treatment with various concentrations of CSF1R inhibitor PLX3397 quantified by CellTiter-Glo assay. Mean ± s.d. of $n = 6$ biological replicates. **l**, Percentage of SPP1$^+$ cells after 24 h of PLX3397 treatment measured via flow cytometry after an additional 5 h of GolgiPlug treatment. In panels **d**, **e**, **g**, **h** and **j**, values represent mean ± s.d. of $n = 3$ biological replicates; in all panels except **i**, *P* values are from the two-tailed Student's *t*-test. i1, i2 refer to independent CRISPRi sgRNAs targeting the indicated genes.

synaptosome phagocytosis in CCL13$^{high}$ cells (representative of the cells in cluster 9) and CCL13$^{low}$ cells (representative of other clusters) in *CDK12* knockdown iTF-Microglia. As observed already in our phagocytosis screen (Fig. 5b), knockdown of *CDK12* decreased synaptosome phagocytosis, in both the CCL13$^{low}$ and CCL13$^{high}$ populations (Fig. 7e). *CDK12* knockdown caused transcriptional downregulation of phosphatidylserine recognition receptors in both CCL13$^{low}$ and CCL13$^{high}$ cells, which may contribute to the decreased phagocytic activity (Extended Data Fig. 9b). Phagocytosis was even further decreased in the CCL13$^{high}$ population (Fig. 7e), suggesting that microglia in the CCL13$^{+}$ state have lower phagocytic capacity, as we showed previously (Fig. 6h). Knockdown of *CDK12* also had some cluster-specific effects (Extended Data Fig. 9b), highlighting the complex effects of gene perturbation in both shifting occupancy of cells between defined functional states, and also affecting cellular pathways in both general and state-specific ways. Interestingly, *MED1* had very similar knockdown phenotypes to *CDK12*, and both genes encode factors associated with general transcription by RNA polymerase II.

We next turned our attention to regulators of the disease-relevant SPP1-positive cluster 3. Knockdown of *MAPK14* and *CSF1R* had dramatically opposing effects, increasing and decreasing occupancy in the SPP1 cluster, respectively (Fig. 7a,b,f). Using GolgiPlug treatment to block secretion of SPP1, we validated these phenotypes by flow cytometry: knockdown of *MAPK14* increased the population of SPP1$^{+}$ cells more than sixfold (Fig. 7g), whereas CSF1R knockdown greatly diminished the proportion of SPP1$^{+}$ cells (Fig. 7h).

Based on these effects of genetic perturbations, we asked if pharmacological targeting of the same hits would similarly modulate the abundance of the SPP1$^{+}$ state. Indeed, inhibition of MAPK14 with Skepinone-L increased the fraction of SPP1$^{+}$ microglia in a time-dependent manner at nontoxic concentrations (Fig. 7i,j)

Given that pharmacological inhibition of CSF1R has shown beneficial effects in several neurodegenerative mouse models, and was observed by us and others to selectively affect subpopulations of microglia in mice[53–55], we tested if pharmacological inhibition of CSF1R would reduce the proportion of SPP1$^{+}$ microglia. While the CSF1R inhibitor PLX3397 showed dose-dependent toxicity in iTF-Microglia (Fig. 7k), low concentrations of CSF1R inhibitor that were nontoxic to bulk iTF-Microglia selectively depleted SPP1$^{+}$ iTF-Microglia (Fig. 7l). Thus, both pharmacological and genetic inhibition of CSF1R can decrease the proportion of SPP1$^{+}$ cells.

In conclusion, our CROP-seq screen enabled deep characterization of the hit genes that our primary screens identified and revealed the existence of a wealth of microglial cell states and their regulators. To enable the scientific community to further explore this large dataset, we implemented additional functionality in the CRISPRbrain data commons (https://www.crisprbrain.org/) we previously described[12]. Specifically, interactive three-dimensional UMAP representations and heatmaps enable the selective investigation of cells by expression levels of genes of interest, sgRNA identity and cluster membership.

## Discussion

In this study, we described a platform for large-scale, multimodal CRISPRi/a-based genetic screens in human iPSC-derived microglia. We demonstrated the power of this platform in multiple large-scale screens. While CRISPR knockout strategies are commonly used for loss-of-function screens, the partial knockdown achieved by CRISPRi enables a more nuanced characterization of the function of essential genes. For example, we uncovered a selective vulnerability of microglia in the SPP1$^{+}$ state to partial knockdown of the microglia-essential gene *CSF1R*. The use of human microglia (as opposed to mouse primary microglia) enabled us to recapitulate microglia features found in human but not mouse brain, such as a state characterized by a chemokine signature[52]. Notwithstanding, there are several areas for future optimization of our iTF-Microglia platform, as detailed in the Supplementary Discussion.

Our platform uncovered insights into microglial biology. We identified several genes associated with neurodegenerative diseases, including *PFN1* and *INPP5D*, as modulators of phagocytosis in microglia (Fig. 5), thus pointing to a possible cellular mechanism by which variants in these genes contribute to disease (Supplementary Discussion).

scRNA-seq revealed that iTF-Microglia adopt a spectrum of states, including states mirroring those observed in human brains. Our CROP-seq screen identified genes controlling the distribution of iTF-Microglia across these states. We demonstrate that knockdown or pharmacological inhibition of MAPK14 or CSF1R promotes or depletes, respectively, the disease-relevant SPP1 state of microglia (Supplementary Discussion). This will make it possible to determine the role of SPP1$^{+}$ microglia in different diseases, where they may play either beneficial or detrimental roles, and to manipulate this disease-associated microglial state for therapeutic benefit.

We anticipate that the screening platform we describe here can be broadly applied to screen for other microglia-related phenotypes, and to systematically identify regulators of different microglial states. Using iPSCs derived from patients with familial or sporadic diseases will enable the identification of potential therapeutic targets that can correct cellular phenotypes[10]. Introduction of microglia into cocultures or brain organoids can provide a screening platform to investigate their interactions with other brain cell types, such as synaptic pruning of neurons. Finally, transplantation of iTF-Microglia into postnatal, immune-deficient, humanized mice could result in microglia with an in vivo human microglial gene signature, including more homeostatic microglia, and enable the investigation of factors controlling the interaction of microglia with a model for diseased brain environment[56–59].

## Online content

Any methods, additional references, Nature Research reporting summaries, source data, extended data, supplementary information, acknowledgements, peer review information; details of author contributions and competing interests; and statements of data and code availability are available at https://doi.org/10.1038/s41593-022-01131-4.

Received: 22 June 2021; Accepted: 24 June 2022;
Published online: 11 August 2022

## References

1. Butovsky, O. & Weiner, H. L. Microglial signatures and their role in health and disease. *Nat. Rev. Neurosci.* **19**, 622–635 (2018).
2. Efthymiou, A. G. & Goate, A. M. Late onset Alzheimer's disease genetics implicates microglial pathways in disease risk. *Mol. Neurodegener.* **12**, 43 (2017).
3. Olah, M. et al. Single cell RNA sequencing of human microglia uncovers a subset associated with Alzheimer's disease. *Nat. Commun.* **11**, 6129 (2020).
4. Mathys, H. et al. Temporal tracking of microglia activation in neurodegeneration at single-cell resolution. *Cell Rep.* **21**, 366–380 (2017).
5. Keren-Shaul, H. et al. A unique microglia type associated with restricting development of Alzheimer's disease. *Cell* **169**, 1276–1290.e17 (2017).
6. Srinivasan, K. et al. Untangling the brain's neuroinflammatory and neurodegenerative transcriptional responses. *Nat. Commun.* **7**, 11295 (2016).
7. Hammond, T. R. et al. Single-cell RNA sequencing of microglia throughout the mouse lifespan and in the injured brain reveals complex cell-state changes. *Immunity* **50**, 253–271.e6 (2019).
8. Masuda, T. et al. Spatial and temporal heterogeneity of mouse and human microglia at single-cell resolution. *Nature* **566**, 388–392 (2019).
9. Sankowski, R. et al. Mapping microglia states in the human brain through the integration of high-dimensional techniques. *Nat. Neurosci.* **22**, 2098–2110 (2019).
10. Kampmann, M. CRISPR-based functional genomics for neurological disease. *Nat. Rev. Neurol.* **16**, 465–480 (2020).
11. Tian, R. et al. CRISPR interference-based platform for multimodal genetic screens in human iPSC-derived neurons. *Neuron* **104**, 239–255 e212 (2019).

12. Tian, R. et al. Genome-wide CRISPRi/a screens in human neurons link lysosomal failure to ferroptosis. *Nat. Neurosci.* **24**, 1020–1034 (2021).
13. Abud, E. M. et al. iPSC-derived human microglia-like cells to study neurological diseases. *Neuron* **94**, 278–293 e279 (2017).
14. Douvaras, P. et al. Directed differentiation of human pluripotent stem cells to microglia. *Stem Cell Rep.* **8**, 1516–1524 (2017).
15. Muffat, J. et al. Efficient derivation of microglia-like cells from human pluripotent stem cells. *Nat. Med.* **22**, 1358–1367 (2016).
16. Pandya, H. et al. Differentiation of human and murine induced pluripotent stem cells to microglia-like cells. *Nat. Neurosci.* **20**, 753–759 (2017).
17. Haenseler, W. et al. A highly efficient human pluripotent stem cell microglia model displays a neuronal-co-culture-specific expression profile and inflammatory response. *Stem Cell Rep.* **8**, 1727–1742 (2017).
18. Brownjohn, P. W. et al. Functional studies of missense TREM2 mutations in human stem cell-derived microglia. *Stem Cell Rep.* **10**, 1294–1307 (2018).
19. McQuade, A. et al. Development and validation of a simplified method to generate human microglia from pluripotent stem cells. *Mol. Neurodegener.* **13**, 67 (2018).
20. Zhang, Y. et al. An RNA-sequencing transcriptome and splicing database of glia, neurons, and vascular cells of the cerebral cortex. *J. Neurosci.* **34**, 11929–11947 (2014).
21. Bennett, M. L. et al. New tools for studying microglia in the mouse and human CNS. *Proc. Natl Acad. Sci. USA* **113**, E1738–E1746 (2016).
22. Hickman, S. E. et al. The microglial sensome revealed by direct RNA sequencing. *Nat. Neurosci.* **16**, 1896–1905 (2013).
23. Bohlen, C. J. et al. Diverse requirements for microglial survival, specification, and function revealed by defined-medium cultures. *Neuron* **94**, 759–773.e8 (2017).
24. Horlbeck, M. A. et al. Compact and highly active next-generation libraries for CRISPR-mediated gene repression and activation. *eLife* **5**, e19760 (2016).
25. Michaelson, M. D. et al. CSF-1 deficiency in mice results in abnormal brain development. *Development* **122**, 2661–2672 (1996).
26. Kondo, Y. & Duncan, I. D. Selective reduction in microglia density and function in the white matter of colony-stimulating factor-1-deficient mice. *J. Neurosci. Res.* **87**, 2686–2695 (2009).
27. Erblich, B., Zhu, L., Etgen, A. M., Dobrenis, K. & Pollard, J. W. Absence of colony stimulation factor-1 receptor results in loss of microglia, disrupted brain development and olfactory deficits. *PLoS ONE* **6**, e26317 (2011).
28. Chitu, V. et al. Microglial homeostasis requires balanced CSF-1/CSF-2 receptor signaling. *Cell Rep.* **30**, 3004–3019 e3005 (2020).
29. Tan, F., Qian, C., Tang, K., Abd-Allah, S. M. & Jing, N. Inhibition of transforming growth factor β (TGF-β) signaling can substitute for Oct4 protein in reprogramming and maintain pluripotency. *J. Biol. Chem.* **290**, 4500–4511 (2015).
30. Butovsky, O. et al. Identification of a unique TGF-β-dependent molecular and functional signature in microglia. *Nat. Neurosci.* **17**, 131–143 (2014).
31. Adler, A. S. et al. CDK8 maintains tumor dedifferentiation and embryonic stem cell pluripotency. *Cancer Res.* **72**, 2129–2139 (2012).
32. Mayo, L. et al. Dual role of CD38 in microglial activation and activation-induced cell death. *J. Immunol.* **181**, 92–103 (2008).
33. Wang, Y. M. et al. Blocking the CD38/cADPR pathway plays a double-edged role in LPS stimulated microglia. *Neuroscience* **361**, 34–42 (2017).
34. Tanzer, M. C., Bludau, I., Stafford, C. A., Hornung, V. & Mann, M. Phosphoproteome profiling uncovers a key role for CDKs in TNF signaling. *Nat. Commun.* **12**, 6053 (2021).
35. Henry, K.L. et al. CDK12-mediated transcriptional regulation of noncanonical NF-κB components is essential for signaling. *Sci. Signal.* **11** (2018).
36. Jin, Z., Wei, W., Yang, M., Du, Y. & Wan, Y. Mitochondrial complex I activity suppresses inflammation and enhances bone resorption by shifting macrophage-osteoclast polarization. *Cell Metab.* **20**, 483–498 (2014).
37. Salter, M. W. & Stevens, B. Microglia emerge as central players in brain disease. *Nat. Med.* **23**, 1018–1027 (2017).
38. Floden, A. M. & Combs, C. K. Microglia demonstrate age-dependent interaction with amyloid-β fibrils. *J. Alzheimers Dis.* **25**, 279–293 (2011).
39. Bliederhaeuser, C. et al. Age-dependent defects of alpha-synuclein oligomer uptake in microglia and monocytes. *Acta Neuropathol.* **131**, 379–391 (2016).
40. Hong, S. et al. Complement and microglia mediate early synapse loss in Alzheimer mouse models. *Science* **352**, 712–716 (2016).
41. Lui, H. et al. Progranulin deficiency promotes circuit-specific synaptic pruning by microglia via complement activation. *Cell* **165**, 921–935 (2016).
42. Gilbert, L. A. et al. Genome-scale CRISPR-mediated control of gene repression and activation. *Cell* **159**, 647–661 (2014).
43. Ramkumar, P. et al. CRISPR-based screens uncover determinants of immunotherapy response in multiple myeloma. *Blood Adv.* **4**, 2899–2911 (2020).
44. Wu, C. H. et al. Mutations in the profilin 1 gene cause familial amyotrophic lateral sclerosis. *Nature* **488**, 499–503 (2012).
45. Schulz, D., Severin, Y., Zanotelli, V. R. T. & Bodenmiller, B. In-depth characterization of monocyte-derived macrophages using a mass cytometry-based phagocytosis assay. *Sci. Rep.* **9**, 1925 (2019).
46. Zou, L. et al. Profilin-1 is a negative regulator of mammary carcinoma aggressiveness. *Br. J. Cancer* **97**, 1361–1371 (2007).
47. Lu, E. et al. Profilin 1 knockdown prevents ischemic brain damage by promoting M2 microglial polarization associated with the RhoA/ROCK pathway. *J. Neurosci. Res.* **98**, 1198–1212 (2020).
48. Masuda, T., Sankowski, R., Staszewski, O. & Prinz, M. Microglia heterogeneity in the single-cell era. *Cell Rep.* **30**, 1271–1281 (2020).
49. Cappellano, G. et al. The *Yin-Yang* of osteopontin in nervous system diseases: damage versus repair. *Neural Regen. Res.* **16**, 1131–1137 (2021).
50. Sala Frigerio, C. et al. The major risk factors for Alzheimer's disease: age, sex, and genes modulate the microglia response to Aβ plaques. *Cell Rep.* **27**, 1293–1306.e6 (2019).
51. Szulzewsky, F. et al. Glioma-associated microglia/macrophages display an expression profile different from M1 and M2 polarization and highly express *Gpnmb* and *Spp1*. *PLoS ONE* **10**, e0116644 (2015).
52. Geirsdottir, L. et al. Cross-species single-cell analysis reveals divergence of the primate microglia program. *Cell* **179**, 1609–1622.e16 (2019).
53. Zhan, L. et al. A MAC2-positive progenitor-like microglial population is resistant to CSF1R inhibition in adult mouse brain. *eLife* **9**, e51796 (2020).
54. Zhan, L. et al. Proximal recolonization by self-renewing microglia re-establishes microglial homeostasis in the adult mouse brain. *PLoS Biol.* **17**, e3000134 (2019).
55. Johnson, N.R. et al. CSF1R inhibitor levels determine sex-specific phenotype of resilient microglia and neurofunctional rescue leading to extended survival in tauopathy mice. Preprint at *bioRxiv* https://doi.org/10.1101/2021.03.20.436288 (2021).
56. Hasselmann, J. et al. Development of a chimeric model to study and manipulate human microglia in vivo. *Neuron* **103**, 1016–1033 e1010 (2019).
57. Mancuso, R. et al. Stem-cell-derived human microglia transplanted in mouse brain to study human disease. *Nat. Neurosci.* **22**, 2111–2116 (2019).
58. Svoboda, D. S. et al. Human iPSC-derived microglia assume a primary microglia-like state after transplantation into the neonatal mouse brain. *Proc. Natl Acad. Sci. USA* **116**, 25293–25303 (2019).
59. Xu, R. et al. Human iPSC-derived mature microglia retain their identity and functionally integrate in the chimeric mouse brain. *Nat. Commun.* **11**, 1577 (2020).
60. Guttikonda, S. R. et al. Fully defined human pluripotent stem cell-derived microglia and tri-culture system model C3 production in Alzheimer's disease. *Nat. Neurosci.* **24**, 343–354 (2021).
61. Chen, S. W. et al. Efficient conversion of human induced pluripotent stem cells into microglia by defined transcription factors. *Stem Cell Rep.* **16**, 1363–1380 (2021).


**Publisher's note** Springer Nature remains neutral with regard to jurisdictional claims in published maps and institutional affiliations.

**Open Access** This article is licensed under a Creative Commons Attribution 4.0 International License, which permits use, sharing, adaptation, distribution and reproduction in any medium or format, as long as you give appropriate credit to the original author(s) and the source, provide a link to the Creative Commons license, and indicate if changes were made. The images or other third party material in this article are included in the article's Creative Commons license, unless indicated otherwise in a credit line to the material. If material is not included in the article's Creative Commons license and your intended use is not permitted by statutory regulation or exceeds the permitted use, you will need to obtain permission directly from the copyright holder. To view a copy of this license, visit http://creativecommons.org/licenses/by/4.0/.

© The Author(s) 2022

## Methods

**Human iPSC culture.** Human iPSCs (male WTC11 background, Coriell Catalog (Cat.) No. GM25256) were cultured in StemFlex Basal Medium (Gibco; Cat. No. A33493-01) on BioLite Cell Culture Treated Dishes (Thermo Fisher Scientific; assorted Cat. Nos.) coated with Growth Factor Reduced, Phenol Red-Free, LDEV-Free Matrigel Basement Membrane Matrix (Corning; Cat. No. 356231) diluted 1:100 in Knockout DMEM (GIBCO/Thermo Fisher Scientific; Cat. No. 10829-018). StemFlex was replaced every other day or every day once 50% confluent. When 70–80% confluent, cells were passaged by aspirating media, washing with DPBS (Gibco; Cat. No. 14190-144), incubating with StemPro Accutase Cell Dissociation Reagent (GIBCO/Thermo Fisher Scientific; Cat. No. A11105-01) at 37 °C for 7 min, diluting Accutase 1:5 in StemFlex, collecting cells in conicals, centrifuging at 220*g* for 5 min, aspirating supernatant, resuspending cell pellet in StemFlex supplemented with 10 nM Y-27632 dihydrochloride ROCK inhibitor (Tocris; Cat. No. 125410), counting and plating onto Matrigel-coated plates at the desired number. Human iPSC studies at the University of California, San Francisco were approved by the Human Gamete, Embryo and Stem Cell Research Committee.

**Human CRISPR iTF-iPS cell line generation.** The two donor plasmids for inducible expression of six codon-optimized transcription factors were constructed using the plasmid pUCM (GENEWIZ). Human iPSCs (WTC11, Coriell Cat. No. GM25256) were engineered to express PU.1, CEBPβ and IRF5 under a doxycycline-inducible system in the CLYBL safe-harbor locus and MAFB, CEBPα and IRF8 in the AAVS1 safe-harbor locus using Transcription Activator-Like Effector Nuclease (TALEN)-based editing as previously described[11]. Clones were selected using both neomycin and puromycin, thus generating the cell line we termed iTF-iPSCs. Next, iTF-iPSCs were transfected with pC13N-dCas9-BFP-KRAB (ref. [11]), pRT029-CLYBL-CAG-DHFR-dCa s9-BFP-KRAB-NLS-DHFR (ref. [11]) or pRT043-CLYBL-DDdCas9VPH-GFP (ref. [12]) to generate constitutive CRISPRi, inducible CRISPRi or inducible CRISPRa iTF-iPS cell lines, respectively, in the CLYBL safe-harbor locus using the same TALEN-editing method. After transfection, BFP-positive (CRISPRi) or GFP-positive (CRISPRa) iTF-iPSCs were repeatedly enriched via FACS (BD FACSAria Fusion).

To generate monoclonal cell lines, 5,000 polyclonal CRISPR iTF-iPSCs were plated on 10-cm dishes to enable isolation of individual clones under direct visualization with an inverted microscope (Evos FL, Thermo Fisher Scientific) in a tissue culture hood via manual scraping. Monoclonal cell lines were tested for iTF-Microglia differentiation capability and CRISPRi/a activity.

**Human iPSC-derived iTF-Microglia cell culture and differentiation.** iTF-iPSCs were grown in StemFlex until reaching at least 50% confluency and were grown for at least 24 h without ROCK inhibitor. They were dissociated and centrifuged as described above and pelleted cells were resuspended in day 0 differentiation medium containing the following: Essential 8 Basal Medium (Gibco; Cat. No. A15169-01) as a base, 10 nM ROCK inhibitor and 2 μg ml$^{-1}$ doxycycline (Clontech; Cat. No. 631311). iTF-iPSCs were counted and seeded onto double-coated plates (Poly-D-Lysine-precoated Bio plates (Corning, assorted Cat. No.) + Matrigel coating) with the following seeding densities: 10,000 cells per well for 96-well plate, 0.1 million per well for 12-well plate, 0.15 million per well for 6-well plate, 2 million per dish for 10-cm dish and 8 million per dish for 15-cm dish. On day 2, medium was replaced with day 2 differentiation medium containing Advanced DMEM/F12 Medium (Gibco; Cat. No. 12634-010) as a base medium containing the following: 1 × Antibiotic-Antimycotic (Anti-Anti) (Gibco; Cat. No. 15240-062), 1 × GlutaMAX (Gibco; Cat. No. 35050-061), 2 μg ml$^{-1}$ doxycycline, 100 ng ml$^{-1}$ Human IL-34 (Peprotech; Cat. No. 200-34) and 10 ng ml$^{-1}$ Human GM-CSF (Peprotech; Cat. No. 300-03). Two days later, on day 4, the medium was replaced with iTF-Microglia medium, containing Advanced DMEM/F12 as a base medium and the following: 1 × Anti-Anti, 1 × GlutaMAX, 2 μg ml$^{-1}$ doxycycline, 100 ng ml$^{-1}$ Human IL-34, 10 ng ml$^{-1}$ Human GM-CSF, 50 ng ml$^{-1}$ Human M-CSF (Peprotech; Cat. No. 300-25) and 50 ng ml$^{-1}$ Human TGFB1 (Peprotech; Cat. No. 100-21C). On day 8, the medium was replaced with fresh iTF-Microglia medium. iTF-Microglia can be cultured for at least 12 more days in iTF-Microglia medium with full medium changes every 3–4 d. Cells were assayed on day 8, day 9 or day 15 in most experiments. When differentiating the inducible CRISPRi/a iTF-Microglia, the medium was supplemented with 50 nM TMP (MP Biomedical; Cat. No. 195527) and changed every 2 d to maintain strong knockdown/overexpression.

For dissociation, iTF-Microglia were washed once with PBS before adding TrypLE Express (Gibco; Cat. No. 12605-028) and incubating for 10 min at 37 °C. Cells were diluted 1:3 in Advanced DMEM/F12 and spun down at 220*g* for 5 min before resuspending in appropriate media.

**Doxycycline removal assay after day 8 of differentiation.** First, 10,000 iTF-iPSCs were seeded into 96-well Flat Clear Bottom White Polystyrene Poly-D-Lysine Coated Microplates (Corning; Cat. No. 3843) and differentiated into iTF-Microglia as described above. At day 8 of the differentiation, the medium of iTF-Microglia was replaced with (1) full media change of iTF-Microglia medium containing 2 μg ml$^{-1}$ doxycycline, or (2) full media change of iTF-Microglia medium containing no doxycycline, or (3) half media changes of iTF-Microglia medium containing no doxycycline. This media-replacing paradigm was repeated every 3 d until day 15. Microglia survival was assessed by performing the CellTiter-Glo 2.0 (Promega; Cat. No. G9242) assay according to the manufacturer's instructions. Luminescence signal was recorded with the M5 plate reader (SpectroMax).

**Differentiation and culture of iPSC-derived microglia following the protocol by Brownjohn and colleagues.** Brownjohn iPSC-Microglia (Brownjohn-iMG) were differentiated from dCas9-KRAB iPSCs (AICS-0090, Coriell Cat. No. AICS-0090-391) using the published protocol[18] with minor modifications. In brief, iPSCs (cultured in StemFlex medium with colonies at 60–80% confluency) were dissociated to single cells with Accutase, collected and plated at 10,000 cells per well in 96-well ultra-low attachment, round bottom plates (Corning; Cat. No. 7007) in 100 μl of embryoid body medium (10 mM ROCK inhibitor, 50 ng ml$^{-1}$ BMP-4 (Peprotech; Cat. No. 120-05), 20 ng ml$^{-1}$ SCF (Peprotech; Cat. No. 300-07) and 50 ng ml$^{-1}$ VEGF (Peprotech; Cat. No. 100-20) in E8 medium), and then subjected to centrifugation at 300*g* for 3 min. Embryoid bodies were cultured for 4 d, with a half medium change after 2 d. On day 4, embryoid bodies were carefully collected and transferred into a 15-ml conical tube, and left to settle at the bottom. The embryoid medium was aspirated and 15–20 embryoid bodies were plated per well in 6-well plates and cultured in 3 ml of hematopoetic medium (2 mM GlutaMax, 1 × Anti-Anti, 55 mM 2-mercaptoethanol (BioRad; Cat. No. 1610710), 100 ng ml$^{-1}$ M-CSF and 25 ng ml$^{-1}$ Human IL-3 (Peprotech; Cat. No. 200-03) in X-Vivo 15 (Lonza; Cat. No. BE02-060F). Two-thirds of the medium was exchanged every 3–4 d. Microglia progenitors were collected from suspension after 14–21 d and plated onto PDL-coated plates in microglia maturation medium (2 mM GlutaMax, 1 × Anti-Anti, 100 ng ml$^{-1}$ IL-34 and 10 ng ml$^{-1}$ GM-CSF in Advanced RPMI-1640 (Gibco; Cat. No. 12633012)). Microglia progenitors were further differentiated for 8 d with full medium change every 2–3 d before using them for experiments.

**iTF-Microglia coculture with iNeurons.** iPSC-derived neurons (iNeurons) were differentiated from WTC11 iPSCs engineered to express NGN2 under a doxycycline-inducible system in the AAVS1 safe-harbor locus as previously described[11,62] with minor modifications as follows: iPSCs were maintained and dissociated as described above and replated on Matrigel-coated dishes in N2 Pre-Differentiation Medium. After 3 d, hereafter day 0, the pre-differentiated neurons were dissociated to single cells with Accutase, collected and plated at 10,000 cells per well in PDL-coated 96-well plates in BrainPhys Neuronal Medium (BrainPhys (STEMCELL Technologies; Cat. No. 05790) as the base, 0.5 × N2 Supplement (Thermo Fisher; Cat. No. 17502-048), 0.5 × B27 Supplement (GIBCO/Thermo Fisher Scientific; Cat. No. 17504-044), 10 ng ml$^{-1}$ NT-3 (PeproTech; Cat. No. 450-03), 10 ng ml$^{-1}$ BDNF, 1 mg ml$^{-1}$ Mouse laminin (Thermo Fisher; Cat. No. 23017-015) and 2 mg ml$^{-1}$ doxycycline. On day 3, a full media change was performed. On day 7, half the medium was removed, and an equal volume of BrainPhys Neuronal Medium was added. On day 14, half the medium was removed and an equal volume of BrainPhys Neuronal Medium containing day 8 iTF-Microglia expressing Lck-mNeonGreen and supplemented with 2× the cytokines of the iTF-Microglia medium was added. Then, 3,000 iTF-Microglia were added to each well and immunostaining experiments were performed after 1 d.

**Lentiviral transduction of iPSCs with sgRNA constructs.** Individual or pooled sgRNAs were lentivirally packaged in HEK293T cells (ATCC Cat. No. CRL-3216) as described[11], and introduced into CRISPRi or CRISPRa iPSCs via lentiviral delivery using TransIT Lenti Reagent (Mirus Bio; Cat. No. MIR 6600) according to manufacturer's protocol. Cells were selected with 2 μg ml$^{-1}$ puromycin (Gibco; Cat. No. A11138-03) for 2–4 d until the fraction of infected cells was > 0.9, as determined by flow cytometry of sgRNA-BFP fluorescence, after which cells were cultured for 2–4 d in the absence of puromycin to allow them to recover. sgRNA protospacer sequences are provided in Supplementary Table 10.

**qPCR.** To quantify *TFRC*, *INPP5D or PICALM* knockdown or *CXCR4, CD209 or PFN1* overexpression, lysed cell pellets from human iPSCs or iTF-Microglia were thawed on ice, and total RNA was extracted using the Quick-RNA Miniprep Kit (Zymo; Cat. No. R1054). Complementary DNA was synthesized with the SensiFAST cDNA Synthesis Kit (Bioline; Cat. No. 65054). Samples were prepared for qPCR in technical triplicates in 5-μl reaction volumes using SensiFAST SYBR Lo-ROX 2X Master Mix (Bioline; Cat. No. BIO-94005), custom qPCR primers from Integrated DNA Technologies used at a final concentration of 0.2 μM and cDNA diluted at 1:3. qPCR was performed on an Applied Biosystems QuantStudio 6 Pro Real-Time PCR System using QuantStudio Real Time PCR software (v.1.3) with the following Fast 2-Step protocol: (1) 95 °C for 20 s; (2) 95 °C for 5 s (denaturation); (3) 60 °C for 20 s (annealing/extension); (4) repeat steps 2 and 3 for a total of 40 cycles; (5) 95 °C for 1 s; (6) ramp 1.92 °C s$^{-1}$ from 60 °C to 95 °C to establish melting curve. Expression fold changes were calculated using the ΔΔCt method, normalizing to housekeeping gene *GAPDH*. Primer sequences are provided in Supplementary Table 10.

**Cell-surface protein staining for flow cytometry.** Dissociated and resuspended iTF-Microglia were blocked for 15 min with 1:20 Human FC Block (BD Biosciences; Cat. No. 564220) and then stained with 1:66 PE/Cy7 anti-human CD184 (CXCR4) (BioLegend; Cat. No. 306514) for CRISPRa validation or 1:66 PE-Cy7 anti-human CD71 (TFRC) (BioLegend; Cat. No. 334112) for CRISPRi validation for 30 min in the dark. For the CD38 screen and validation experiments, iTF-Microglia were stained with 1:200 anti-hCD38 PE (R&D Systems; Cat. No. FAB2404P). Cells were washed twice with DPBS before analyzing them by flow cytometry using the BD LSRFortessa X14 (BD Biosciences) using BD FACSDiva (v.8.0.1.1) software. Flow cytometry data were analyzed using FlowJo (FlowJo, v.10.7.1); raw median fluorescence intensity values of CD184, CD71 and CD38 stained cells were normalized to nonstained control samples; and data were plotted as fold change using Prism 8 (GraphPad, v.8.4.2).

**Intracellular protein staining for flow cytometry.** iTF-Microglia were treated for 6 h with 1:2,000 GolgiPlug (BD; Cat. No. 555029) or dimethylsulfoxide as control before dissociating. Cells were fixed and permeabilized with the eBioscience Intracellular Fixation and Permeabilization Buffer Set (Invitrogen; Cat. No. 88-8824-00) according to the manufacturer's instructions. Cells were stained with 1:75 Anti-Hu Osteopontin (SPP1) eFluor 660 (eBioscience; Cat. No. 50-9096-42) or 1:75 Human CCL13 488 (R&D Systems; Cat. No. IC327G) or their isotype controls Mouse IgG1 Control Alexa Fluor 488 conjugated (R&D Systems; Cat. No. IC002G) and Mouse IGG1 kappa Isotype (eBioscience; Cat. No. 50-4714-82) overnight at 4 °C. Cells were washed twice with DPBS before analyzing them by flow cytometry using the BD FACS Celesta (BD Biosciences) or the BD FACSAria Fusion using BD FACSDiva (v.8.0.1.1) software. Flow cytometry data were analyzed using FlowJo, raw median fluorescence intensity values of Osteopontin (SPP1) and CCL13 stained cells were normalized to isotype-control samples and data were plotted as fold change using Prism 8. The gating strategy used to determine the percentage of SPP1-positive cells is shown in Supplementary Fig. 1c.

**Immunohistochemistry.** iTF-Microglia monocultures and cocultures were differentiated in PDL-coated 96-well plates. They were fixed with 4% paraformaldehyde (Electron Microscopy Sciences; Cat. No. 15710) for 10 min at room temperature. After washing with DPBS three times, cells were permeabilized and blocked with 5% normal goat serum (Vector Laboratories; Cat. No. S-1000-20) with 0.01% Triton X-100 (TEKnova; Cat. No. T1105) in PBS for 1 h at room temperature. Cells were then incubated with primary antibodies diluted in blocking buffer at 4 °C overnight. After that, cells were washed with DPBS three times and incubated with secondary antibodies diluted in blocking buffer for 1 h at room temperature. Cells were then washed with DPBS three times and stained with 10 μg ml$^{-1}$ Hoechst 33342 (Thermo Fisher Scientific; Cat. No. H3570) for 10 min. Cells were imaged using a confocal microscope (Leica SP8) or an IN Cell Analyzer 6000 (GE; Cat. No. 28-9938-51) using IN Cell Analyzer 6000 Acquisition Software (v.4.0). Primary antibodies used for immunofluorescence in this study were as follows: anti-mouse 1:150 GPR34 (R&D Systems; Cat. No. MAB4617), anti-rabbit 1:1,000 IBA1 (Wako; Cat. No. 019-19741), anti-rabbit 1:200 TFRC (abcam; Cat. No. ab84036), anti-rabbit 1:1,000 synaptophysin (Synaptic Systems; Cat. No. 101 004). Secondary antibodies used in this study were as follows: goat anti-rabbit IgG Alexa Fluor 555 (1:500 dilution; abcam; Cat. No. ab150078), goat anti-mouse IgG Alexa Fluor 488 (1:500 dilution; abcam; Cat. No. ab150113) and goat anti-chicken IgG Alexa Fluor 647. F-actin was stained using ActinGreen 488 (Invitrogen; Cat. No. R37110) according to the manufacturer's protocol.

**Synaptosome isolation and pHrodo-Red labeling.** Synaptosomes were isolated from fresh Innovative Grade US Origin Rat Sprague Dawley Brain (Innovative Research; Cat. No. IGRTSDBR) with the Syn-PER Synaptic Protein Extraction Reagent (Thermo Scientific; Cat. No. 87793) according to the manufacture's protocol with minor changes. Briefly, 10 ml of Syn-PER Reagent supplemented with 1× protease inhibitor cOmplete Mini, EDTA free (Roche; Cat. No. 11836170001) and 1× phosphatase inhibitor PhosSTOP (Roche; Cat. No. 4906845001) were added per gram of brain tissue. Dounce homogenization was performed on ice and homogenate was transferred to a conical tube and centrifuged at 1,200*g* for 10 min at 4 °C. The pellet was discarded, the supernatant was transferred to a new tube and the centrifugation step was repeated. The supernatant was then centrifuged at 15,000*g* for 20 min at 4 °C. The supernatant was removed and the wet pellet was weighed. The synaptosome fractions were resuspended at a concentration of 50 mg ml$^{-1}$. Then, 3 μM pHrodo-Red, succinimidyl ester (Thermo Fisher Scientific; Cat. No. P36600) was added to the synaptosome fraction and incubated for 45 min at room temperature in the dark. After diluting the solution 1:10 in DPBS, the synaptosomes were spun down at 2,500*g* for 5 min. The supernatant was removed and then the synaptosomes were washed two times with DPBS. The pHrodo-labeled synaptosomes were resuspended in iTF-Microglia medium at a stock concentration of 50 mg ml$^{-1}$ and directly used for phagocytosis assays or frozen in synaptosome freezing medium (5% dimethylsulfoxide in Advanced DMEM/F12) for later use.

**Phagocytosis assays.** Day 8 iTF-Microglia were used for all phagocytosis assays. iTF-Microglia medium was prepared with pHrodo-Red-labeled synaptosomes at a concentration of 1 mg ml$^{-1}$ or 0.5 μl ml$^{-1}$ media of Fluoresbrite Carboxylate YG 1.0 Micron Microspheres (15702-10; Cat. No. 15702-10). After replacing the media with the substrate media, iTF-Microglia were incubated for 1.5 h in the incubator if not otherwise stated. Cells were washed twice with DPBS, dissociated, resuspended in ice-cold DPBS and analyzed via flow cytometry. Where indicated, actin polymerization was inhibited by pretreating cells with 5 μM Cytochalasin D (Invitrogen; Cat. No. PHZ1063) for 30 min before the addition of phagocytic substrate media. For analyzing phagocytic capabilities within microglia clusters, pHrodo-Red-labeled synaptosomes at a concentration of 1 mg ml$^{-1}$ were added to iTF-Microglia for 1.5 h. Microglia were washed three times with PBS before incubating them in iTF-Microglia media supplemented with 1:2,000 GolgiPlug (BD; Cat. No. 555029) for 4 h. Cells were dissociated, fixed and stained for CCL13 and SPP1 as described above. Flow cytometry data were analyzed using FlowJo, raw median fluorescence intensity values of phagocytosing cells were normalized to no-substrate control samples and data were plotted as fold change using Prism 8.

**Human cytokine array.** Day 8 iTF-Microglia were treated with 100 ng ml$^{-1}$ LPS (Millipore Sigma; Cat. No. LPS25) or DPBS control. After 24 h, the supernatant was collected and processed using the Proteome Profiler Human Cytokine Array Kit (R&D Systems; Cat. No. ARY005B), according to the manufacturer's instructions. Data were acquired using Image Studio (v.5.2). For analysis of the signals, Fiji (v.2.0.0) was used to measure the integrated pixel density for each pair of duplicate dots representing a cytokine. Background signal was measured from negative control dots and then subtracted from each dot. The relative change in cytokine levels as a result of LPS treatment was obtained by comparing corresponding cytokine signals across multiple arrays performed in tandem.

**Live-cell imaging.** iTF-iPSCs transduced with individual sgRNAs as described above were passaged and differentiated into iTF-Microglia in the 96-well format described above. Starting on day 2 of differentiation, and continuing every 2 d until day 15, iTF-Microglia were stained with 10 μg ml$^{-1}$ Hoechst 33342 for 10 min at 37 °C, washed with PBS and imaged with the IN Cell Analyzer 6000 using IN Cell Analyzer 6000 Acquisition Software (v.4.0). Using the same 96-well format as described above, day 8 iTF-Microglia were stained for F-actin using 25 nM SiR-actin (Cytoskeleton; Cat. No. CY-SC001) probe diluted in iTF-Microglia medium, with a 4-h incubation at 37 °C. A full media change with iTF-Microglia medium was completed before imaging using the IN Cell Analyzer 6000.

**CellTiter-Glo assay after pharmaceutical inhibition of CSF1R or MAPK14.** First, 10,000 iTF-iPSCs were seeded into 96-well Flat Clear Bottom White Polystyrene Poly-D-Lysine Coated Microplates (Corning; Cat. No. 3843) and differentiated into iTF-Microglia. For CSF1R inhibition, cells were treated with the CSF1R inhibitor PLX3397 at day 8 (ApexBio; Cat. No. B5854) at indicated concentrations or dimethylsulfoxide control for 24 h before performing the CellTiter-Glo 2.0 (Promega; Cat. No. G9242) assay according to the manufacturer's instructions. For MAPK14 inhibition, cells were treated with the MAPK14 inhibitor Skepinone-L at day 8 (Selleckchem; Cat. No. 1221485831) at indicated concentrations or dimethylsulfoxide control for 24 h before performing the CellTiter-Glo 2.0 assay. Luminescence signal was recorded with the M5 plate reader (SpectroMax) using SoftMax Pro 6.5.1.

**CRISPR screens.** *Large-scale survival-based and FACS-based screens.* Inducible CRISPRi and CRISPRa iTF-iPSCs were infected with pooled CRISPRi or CRISPRa sgRNA libraries[24] targeting the druggable genome and selected for lentiviral integration with puromycin, as described above. Day 0 iTF-iPSCs, with a cell count corresponding to an average 1,000× coverage per library element, were differentiated into iTF-Microglia as described above, with constant TMP supplementation for dCas9 stabilization.

For the survival screens, day 0 iPSCs and day 15 iTF-Microglia were lifted with Accutase or TryplE Express, respectively. Lifted cells were collected and subjected to sample preparation for next-generation sequencing as described below.

For the CD38-activation screen, day 8 iTF-Microglia were dissociated with TryplE and then blocked and stained with anti-PE-CD38 as described in the cell-surface staining section. Cells were sorted into high- and low-signal populations corresponding to the top 30% and the bottom 30% of the CD38-PE signal distribution (gating strategy shown in Supplementary Fig. 1a).

For the phagocytosis FACS screen, day 15 iTF-Microglia were incubated with PhRodo-Red synaptosomes as described in the phagocytosis assay section. Cells were then dissociated with TryplE and sorted into high- and low-signal populations corresponding to the top 30% and the bottom 30% of the PhRodo-Red signal distribution (gating strategy shown in Supplementary Fig. 1b). Based on simulations, we previously found that this sorting strategy is optimal for hit detection in FACS-based screens[63].

Cells were subjected to sample preparation for next-generation sequencing as previously described[11]. Briefly, for each screen sample, genomic DNA was isolated using a Macherey-Nagel Blood L kit (Macherey-Nagel; Cat. No. 740954.20). sgRNA-encoding regions were amplified and sequenced on an Illumina HiSeq-4000.

*QuantSeq.* Cell culture medium was aspirated, cells were washed once with DPBS and RNA lysis buffer was added directly to wells containing day 0 iTF-iPSCs, day 15 iTF-Microglia + 50 ng ml$^{-1}$ 24-h LPS treatment, Brownjohn-iMG + 100 ng ml$^{-1}$ 24-h LPS treatment or day 15 iTF-Microglia. For assessing transcriptomic effects after *PFN1* overexpression, two different *PFN1* sgRNAs and NTC sgRNAs were transduced into inducible CRISPRa iPSCs and cells were differentiated to day 8 iTF-Microglia. Biological triplicates for each condition (approximately 0.15 million cells each) were pelleted, snap frozen and stored at −80 °C. RNA was extracted using the Quick-RNA Miniprep Kit (Zymo; Cat. No. R1055). Libraries were prepared from total RNA (250–473 ng per sample) using the QuantSeq 3′ mRNA-Seq Library Prep Kit for Illumina (FWD) (Lexogen; Cat. No. 015UG009V0252) following the manufacturer's instructions. Library amplification was performed with 14 total PCR cycles. mRNA-Seq library concentrations (mean of 1.13 ± 0.66 ng µl$^{-1}$) were measured with the Qubit dsDNA HS Assay Kit (Invitrogen; Cat. No. Q32851) on a Qubit 2.0 Fluorometer. Library fragment-length distributions (mean of 287 ± 28 base pairs) were quantified with High Sensitivity D5000 Reagents (Agilent Technologies; Cat. No. 5067-5593) on the 4200 TapeStation System. The libraries were sequenced on an Illumina NextSeq 2000 instrument with single-end reads.

*CROP-seq.* A pooled sgRNA library consisting of two sgRNAs per targeted gene and four NTC sgRNAs was designed to target 39 genes which were selected hit genes from iTF-Microglia survival and FACS-based screens (Supplementary Table 5; only one sgRNA for gene *DBF4* due to technical error). Briefly, top and bottom strands of sgRNA oligos were synthesized (Integrated DNA Technologies) and annealed in an arrayed format, pooled in equal amounts and ligated into our optimized CROP-seq vector, as previously described[11].

Inducible CRISPRi iTF-iPSCs were infected with the pooled sgRNA library at <0.15 MOI and then selected for lentiviral integration. Next, iTF-iPSCs were differentiated into iTF-Microglia and cultured with the addition of TMP. Day 8 iTF-Microglia were washed three times with DPBS, dissociated with TrypLE and resuspended in nuclease-free water before loading onto four wells of the 10x Chromium Controller (10X Genomics, v.3.1) according to the manufacturer's protocol, with 35,000 cells recovered per sample as the target. Sample preparation was performed using the Chromium Next GEM Single Cell 3′ Reagent Kits v.3.1 (10X Genomics, Cat. No. PN-1000121) according to the manufacturer's protocol, reserving 10–30 ng of full-length cDNA to facilitate sgRNA assignment by amplifying sgRNA-containing transcripts using hemi-nested PCR reactions adapted from a previously published approach[11,64]. cDNA fragment analysis was performed using the 4200 TapeStation System and sgRNA enrichment libraries were separately indexed and sequenced as spike-ins alongside the whole-transcriptome scRNA-seq libraries using a NovaSeq 6000 using the following configuration: Read 1: 28; i7 index: 8; i5 index: 0; Read 2: 91.

**Computational and statistical analysis.** *Primary CRISPR screen analysis.* Primary screens were analyzed using our previously published MAGeCK-iNC bioinformatics pipeline[11], available at https://kampmannlab.ucsf.edu/mageck-inc. Briefly, raw sequencing reads from next-generation sequencing were cropped and aligned to the reference using Bowtie v.0.12.9 (ref. [65]) to determine sgRNA counts in each sample. The quality of each screen was assessed by plotting the $\log_{10}$(counts) per sgRNA on a rank order plot using ggplot2 v.3.3.3 (ref. [66]). Raw phenotype scores and significance *P* values were calculated for target genes, as well as for 'negative-control-quasi-genes' that were generated by random sampling with replacement of five NTC sgRNAs from all NTC sgRNAs. The final phenotype score for each gene was calculated by subtracting the raw phenotype score by the median raw phenotype score of 'negative-control-quasi-genes' and then dividing by the standard deviation of raw phenotype scores of 'negative-control-quasi-genes'.

A 'Gene Score' was defined as the product of phenotype score and $-\log_{10}$(P value). Hit genes were determined based on the Gene Score cut-off corresponding to an empirical false discovery rate of 10%. Volcano plots of Gene Scores were generated using ggplot2 v.3.3.3 (ref. [66]).

*RNA-seq analysis.* Alignment and mapping were performed using Salmon v.1.4.0 (ref. [67]) (the --noLengthCorrection flag was used for QuantSeq samples) and either the human reference genome GRCh38 (Gencode, release 37), or a custom GRCh38 reference genome containing the references for each 3TF transgene integrated in iTF-iPSCs, to obtain transcript abundance counts. Tximport v.1.18.0 (ref. [68]) was used to obtain gene-level count estimates. Genes with zero counts across all samples were removed from the analysis. To visualize differences in gene expression across samples, a list of gene symbols corresponding to microglia markers, microglia activation markers and iPSC markers was compiled from a previous publication[56]; the normalized counts of each of these genes were then standardized across samples (that is, subtracting by the mean and dividing by the standard deviation) and visualized using Complex Heatmap v.2.6.2 (ref. [69]). To assess how iTF-Microglia compare to other iPSC-Microglia and primary microglia from a range of previous studies[13,18,20,60,61], raw fastqs (obtained from the NCBI GEO database) were subjected to the same analysis pipeline stated above. Then, principal component analysis was performed using microglial marker genes as input with DESeq2 v.1.30.1 (ref. [70]). For differential gene expression analysis of LPS-treated versus PBS-treated iTF-Microglia samples and the *PFN1* overexpression versus NTC iTF-Microglia, DESeq2 v.1.30.1 (ref. [70]) was used to calculate the log-fold change and *P* values and to perform shrinkage of log-fold change for downstream visualization using ggplot2 v.3.3.3 (ref. [66]). To compare both LPS-treatment upregulated and downregulated DEGs in iTF-Microglia and Brownjohn-iMG, DEGs that were significant ($P_{adj} < 0.05$) in at least one cell type were visualized using VennDiagram (v.1.6.20).

*CROP-seq analysis.* Alignment and gene expression quantification were performed on scRNA-seq libraries and sgRNA-enriched libraries using Cell Ranger (v.5.0.1, 10X Genomics) with default parameters and reference genome GRCh38-3.0.0. Cellranger aggr was used to aggregate counts belonging to the same sample across different GEM wells. The resulting gene versus cell barcode matrix contained 58,302 cells which had on average 41,827 reads per cell, and a median of 3,346 genes per cell. sgRNA unique molecular identifier counts for each cell barcode were obtained using a previously described mapping workflow[64]. To facilitate sgRNA identity assignment, a combination of demuxEM[71] and a z-score cut-off method we previously described[11] were used such that only cells with a single sgRNA as determined by both methods were carried forward in the analysis.

The raw gene versus barcode matrix outputted by Cell Ranger was converted into a SingleCellExperiment (SCE) object using the read10xCounts function from the DropletUtils package v.1.10.3 (ref. [72]) in R (v.4.0.3). sgRNA assignments were appended to the SCE metadata and filtered to only include cells with a single sgRNA, resulting in 28,905 cells. The SCE was converted into a Seurat object using Seurat::as.Seurat v.4.0.1 (ref. [73]). The data were normalized and highly variable genes were identified using Seurat::SCTransform[74]. For initial data exploration, principal component analysis was performed using Seurat::RunPCA to determine the number of principal components to retain. UMAP dimensional reduction using Seurat::RunUMAP and clustering using Seurat::FindNeighbors and Seurat::FindClusters were performed on the retained principal components, with resolution = 0.7.

Initial data exploration revealed clusters that were not of interest due to a high proportion of mitochondrial-encoding genes or disrupted microglia differentiation (Extended Data Fig. 5a). These clusters were removed from the downstream analysis and the remaining 'microglia cluster' population was normalized, clustered and visualized using UMAP, as described above, with resolution = 0.25.

To determine the DEGs between UMAP clusters, Seurat::FindAllMarkers was used. Single-cell heatmaps, ridge plots, rank plots and UMAPs were made using Seurat::DoHeatmap, Seurat::RidgePlot, Seurat::VizDimLoadings, and Seurat::DimPlot or Seurat::FeaturePlot, respectively.

The relative proportion of cells with a given sgRNA in a given cluster compared with cells with NTC sgRNAs in the given cluster was calculated and visualized using Complex Heatmap v.2.6.2 (ref. [69]) (Supplementary Table 7).

For each CRISPRi target gene, the population of cells with the strongest knockdown (cells with expression of target gene less than the median expression of the target gene) was carried forward to perform differential gene expression analysis using Seurat::FindMarkers with parameters test.use = 't' (student's *t*-test), assay = 'SCT', slot = 'scale.data', to compare the Pearson residuals of cells[74] with knockdown sgRNAs versus NTC cells. Genes with an adjusted $P < 0.1$ were deemed significant. The top 20 DEGs for each target gene which had >50 cells comprised the set of genes used to visualize convergent pathways using Complex Heatmap v.2.6.2 (ref. [69]).

The iTF-Microglia CROP-seq dataset was integrated with the previously published human scRNA-seq dataset (Olah-hMG)[3] using Seurat[75]. Briefly, the Olah-hMG gene versus cell barcode matrix and metadata were used to create a Seurat object and cells from surgery samples or with nonmicroglia identities as previously determined[3] were removed. Normalization and identification of highly variable genes were performed using Seurat::SCTransform with the same parameters as the iTF-Microglia. Next, integration features (3,000 features) and integration anchors were identified for each Seurat object using Seurat::SelectIntegrationFeatures and Seurat::FindIntegrationAnchors and subsequent integration with identified anchors was performed using Seurat::IntegrateData. The integrated Seurat object was normalized, clustered and visualized using UMAP, as described above, with resolution = 0.25. Gene expression was visualized with UMAP using Seurat::FeaturePlot and the percentage of cells in the integrated SPP1-high cluster or SPP1-low clusters of either AD brain or control brain origin was calculated and significance was calculated on the cell counts using Fisher's exact test.

**Image analysis with CellProfiler.** Pipelines and example images are compiled in supplementary material and all analyses were performed using CellProfiler v.4.1.3. Cell morphology metrics: Nuclei were segmented as primary objects from Hoechst images. Cell segmentations were generated by propagating outward from nuclei objects until edges were identified in the phalloidin images. Area and shape metrics were calculated for each cell object. Integrated F-actin intensity per cell: For a given field of view, nuclei were segmented based on Hoechst images and total integrated SiR-actin intensity was summed. The resulting sum was divided by the number of nuclei. Longitudinal cell counts: For a given field of view, nuclei were segmented based on Hoechst images acquired daily. IBA1 intensity per cell: This metric was determined similarly to the integrated F-actin intensity per nucleus; for a given

field of view, the total integrated intensity of the IBA1 stain was divided by the number of segmented nuclei based on Hoechst.

*Statistics and reproducibility.* No statistical methods were used to pre-determine sample sizes but our sample sizes are similar to those reported in previous publications[11,12]. No randomization of samples was used since treatment group of cells were generally derived from the same population of cells. Data collection and analysis were not performed blind to the conditions of the experiments. No data points were excluded from analysis. Data distribution was assumed to be normal but this was not formally tested. For all imaging experiments (Figs. 1b,d, 2a,c,f and 3d and Extended Data Fig. 1a), similar results were observed in $n = 3$ independent experiments.

**Reporting summary.** Further information on research design is available in the Nature Research Reporting Summary linked to this article.

## Data availability

All screen datasets and RNA transcriptomic datasets are publicly available in the CRISPRbrain data commons (http://crisprbrain.org/) (associated with Figs. 1, 2, 4, 5, 6 and 7 and Extended Data Figs. 1, 4, 5, 6 and 7). RNA-sequencing datasets reported in this paper are available on NCBI GEO, accession number GSE178317 (https://www.ncbi.nlm.nih.gov/geo/query/acc.cgi?acc=GSE178317). There are no restrictions on data availability.

## Code availability

The MAGeCK-iNC bioinformatics pipeline for analysis of pooled screens is available at https://kampmannlab.ucsf.edu/mageck-inc. The R notebooks for the RNA-seq and CROP-seq analyses are available at https://kampmannlab.ucsf.edu/article/microglia-analysis. The CellProfiler pipelines will be made available on request to the corresponding authors (M.K.), and will also be submitted to the CellProfiler depository of published pipelines (https://cellprofiler.org/examples/published_pipelines.html) upon publication.

## References


62. Wang, C. et al. Scalable production of iPSC-derived human neurons to identify tau-lowering compounds by high-content screening. *Stem Cell Rep.* **9**, 1221–1233 (2017).
63. Nagy, T. & Kampmann, M. CRISPulator: a discrete simulation tool for pooled genetic screens. *BMC Bioinform.* **18**, 347 (2017).
64. Hill, A. J. et al. On the design of CRISPR-based single-cell molecular screens. *Nat. Methods* **15**, 271–274 (2018).
65. Langmead, B., Trapnell, C., Pop, M. & Salzberg, S. L. Ultrafast and memory-efficient alignment of short DNA sequences to the human genome. *Genome Biol.* **10**, R25 (2009).
66. Wickham, H. ggplot2 Elegant Graphics for Data Analysis (Springer International Publishing, 2016).
67. Patro, R., Duggal, G., Love, M. I., Irizarry, R. A. & Kingsford, C. Salmon provides fast and bias-aware quantification of transcript expression. *Nat. Methods* **14**, 417–419 (2017).
68. Soneson, C., Love, M. I. & Robinson, M. D. Differential analyses for RNA-seq: transcript-level estimates improve gene-level inferences. *F1000Res* **4**, 1521 (2015).
69. Gu, Z., Eils, R. & Schlesner, M. Complex heatmaps reveal patterns and correlations in multidimensional genomic data. *Bioinformatics* **32**, 2847–2849 (2016).
70. Love, M. I., Huber, W. & Anders, S. Moderated estimation of fold change and dispersion for RNA-seq data with DESeq2. *Genome Biol.* **15**, 550 (2014).
71. Gaublomme, J. T. et al. Nuclei multiplexing with barcoded antibodies for single-nucleus genomics. *Nat. Commun.* **10**, 2907 (2019).
72. Lun, A. T. L. et al. EmptyDrops: distinguishing cells from empty droplets in droplet-based single-cell RNA sequencing data. *Genome Biol.* **20**, 63 (2019).
73. Hao, Y. et al. Integrated analysis of multimodal single-cell data. *Cell* **184**, 3573–3587 (2021).
74. Hafemeister, C. & Satija, R. Normalization and variance stabilization of single-cell RNA-seq data using regularized negative binomial regression. *Genome Biol.* **20**, 296 (2019).
75. Stuart, T. et al. Comprehensive integration of single-cell data. *Cell* **177**, 1888–1902.e21 (2019).


## Acknowledgements


We thank R. Tian for discussions about CROP-seq; C. Bohlen for advice on synaptosome protocols; and J. Mella, K. Vivanco, C. Rinaldi, G. Sturm, Y. Li, C. Condello and M. Sullivan for contributions to preliminary studies. We thank A. Samelson for feedback on the manuscript and members of the Kampmann laboratory for discussions. This research was supported by NIH grants no. DP2 GM119139 and no. U01 MH115747 to M.K., no. U54 NS100717 to L.G. and M.K., no. R01 AG051390 to L.G., no. F30 AG066418 to K.L. and no. F30 AG062043 to L.K.; was funded by the Center for Alzheimer's and Related Dementias (CARD) of the National Institutes of Health (NIH) under Award Number ZO1 AG000534-02; and was funded, in part, through the Intramural Research Program of the National Institutes of Neurological Disorders and Stroke (M.E.W.). The research was also supported by an NSF Graduate Research Fellowship to O.M.T.; Tau Consortium Investigator Awards (Rainwater Charitable Foundation) to J.I., L.G. and M.K.; and a Chan Zuckerberg Initiative Ben Barres Early Career Acceleration Award and a Chan Zuckerberg Biohub Investigator Award to M.K. Development of new features for CRISPRbrain was supported, in part, by a collaboration among the Kampmann Lab, UCSF and Data Tecnica International, LLC, and by funding from the Center for Alzheimer's and Related Dementias, National Institutes of Health. The funders had no role in study design, data collection and analysis, decision to publish or preparation of the manuscript.


## Author contributions

The iTF-Microglia differentiation strategy was developed and characterized by C.T.-L.H. and L.G. with contributions from C.D.C., L.Z., J.C.U., L.K., J.I. and M.E.W. Additionally, N.M.D., S.M.S., O.M.T., K.L., J.H. and M.K. contributed to the optimization and characterization of iTF-Microglia. CRISPR-based functional genomics studies were designed, conducted and analyzed by N.M.D., S.M.S. and M.K. with contributions from O.M.T., K.L., G.A. and J.H. S.M.S. led the computational analysis of all screens and RNA-seq experiments. S.H.H. and F.F. developed new features for the CRISPRbrain data commons with critical input from S.M.S., N.M.D. and M.K. and feedback from M.A.N. and A.B.S. N.M.D., S.M.S., C.T.-L.H., O.M.T. and M.K. created the figures. N.M.D., S.M.S. and M.K. conceptualized and wrote the manuscript with input from the other authors. All authors reviewed and approved the final manuscript.

## Competing interests

M.A.N. consults for Neuron23. M.A.N. and F.F. participated in this work in part due to a competitively awarded consulting contract between Data Tecnica International, LLC and the National Institutes of Health (USA). J.I. is a cofounder of AcuraStem, Inc. and Modulo Bio, and serves on the scientific advisory board of Spinogenix. L.G. is a founder of Aeton Therapeutics. M.K. is an inventor on US patent 11,254,933 related to CRISPRi and CRISPRa screening; serves on the scientific advisory boards of Engine Biosciences, Casma Therapeutics, Cajal Neuroscience and Alector; and is a consultant to Modulo Bio and Recursion Therapeutics. The remaining authors declare no competing interests.

## Additional information

**Extended data** is available for this paper at https://doi.org/10.1038/s41593-022-01131-4.

**Supplementary information** The online version contains supplementary material available at https://doi.org/10.1038/s41593-022-01131-4.

**Correspondence and requests for materials** should be addressed to Li Gan or Martin Kampmann.

**Peer review information** *Nature Neuroscience* thanks Mathew Blurton-Jones and the other, anonymous, reviewer(s) for their contribution to the peer review of this work. This article has been peer reviewed as part of Springer Nature's Guided Open Access initiative. Peer reviewer reports are available.

**Reprints and permissions information** is available at www.nature.com/reprints.

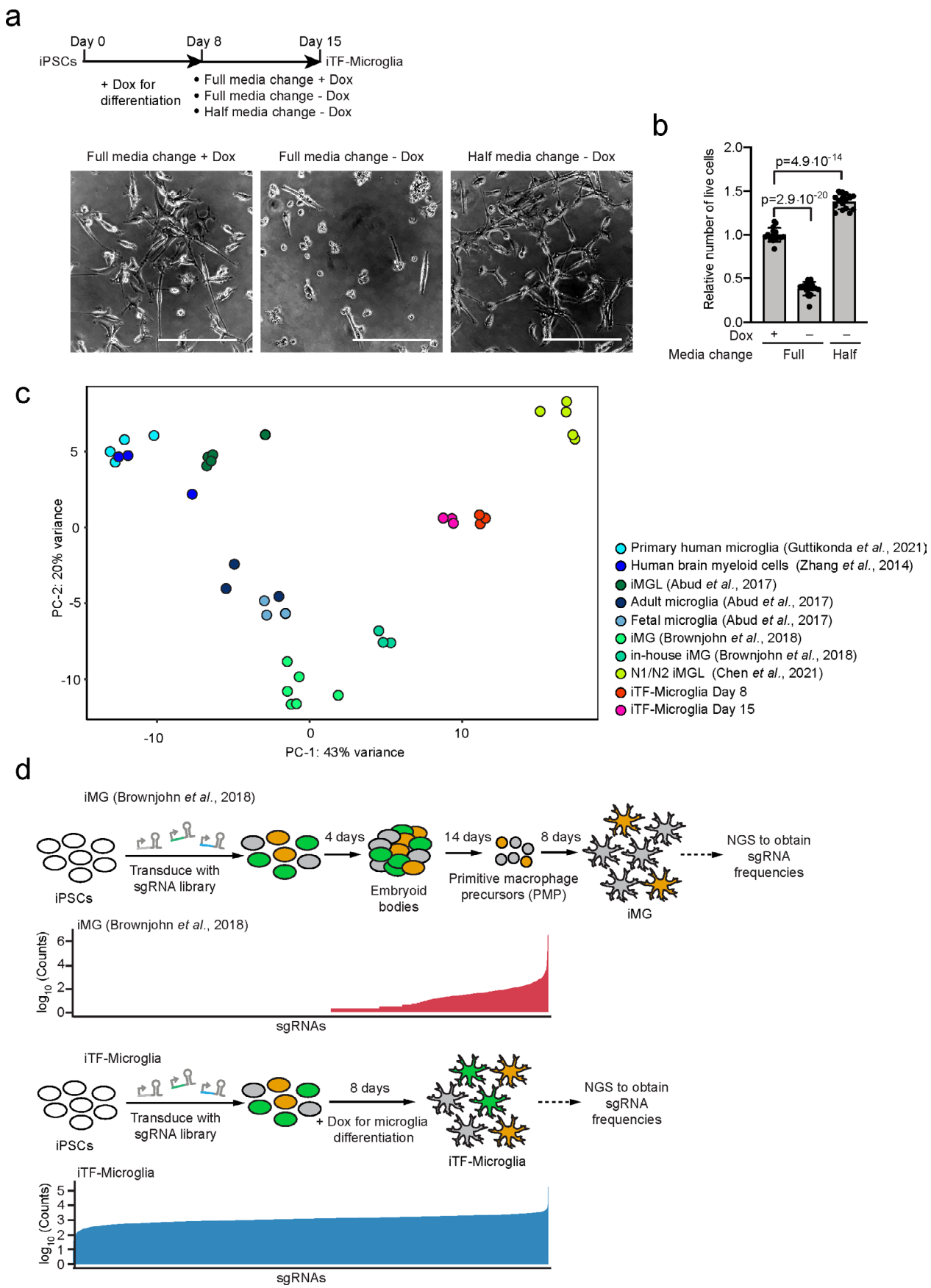


**Extended Data Fig. 1 | See next page for caption.**

**Extended Data Fig. 1 | Impact of Doxycycline removal on iTF-Microglia survival and sgRNA recovery in iPSC-derived microglia generated with different protocols. a**, Comparison of iTF-Microglia viability after Day 8 with different protocols. *Top*: timeline with different doxycycline supplementation paradigms, *bottom*: representative phase-contrast images at Day 15 with the indicated doxyccycline supplementation. Scale bar: 50 µm. **b**, Survival of iTF-Microglia at Day 15 after different doxycycline treatments indicated in a. Viable cells were quantified using the CellTiter-Glo assay. Values represent mean +/− sd of n = 12 biological replicates; p values from two-tailed Student's t-test. **c**, Principal component analysis (PCA) on the expression of microglia marker genes of iTF-Microglia, human adult ex-vivo microglia[60], fetal and adult microglia[13], human myeloid cells[20], other iPSC-microglia[13,18,61]. No iPSC samples were included. Each dot reflects an independent biological sample. Colors represent the different cell types. **d**, sgRNA recovery after transduction with a pooled sgRNA library in iPSCs and differentiation with two different iPSC-Microglia protocols. Strategy for the infection of iPSCs with an sgRNA library with 13,025 elements and timepoint of sgRNA recovery in iPSC-Microglia with the actual recovered counts of sgRNAs after next-generation-sequencing (NGS) from the protocol from Brownjohn *et al.*[18] (*Top*) and iTF-Microglia (*Bottom*).

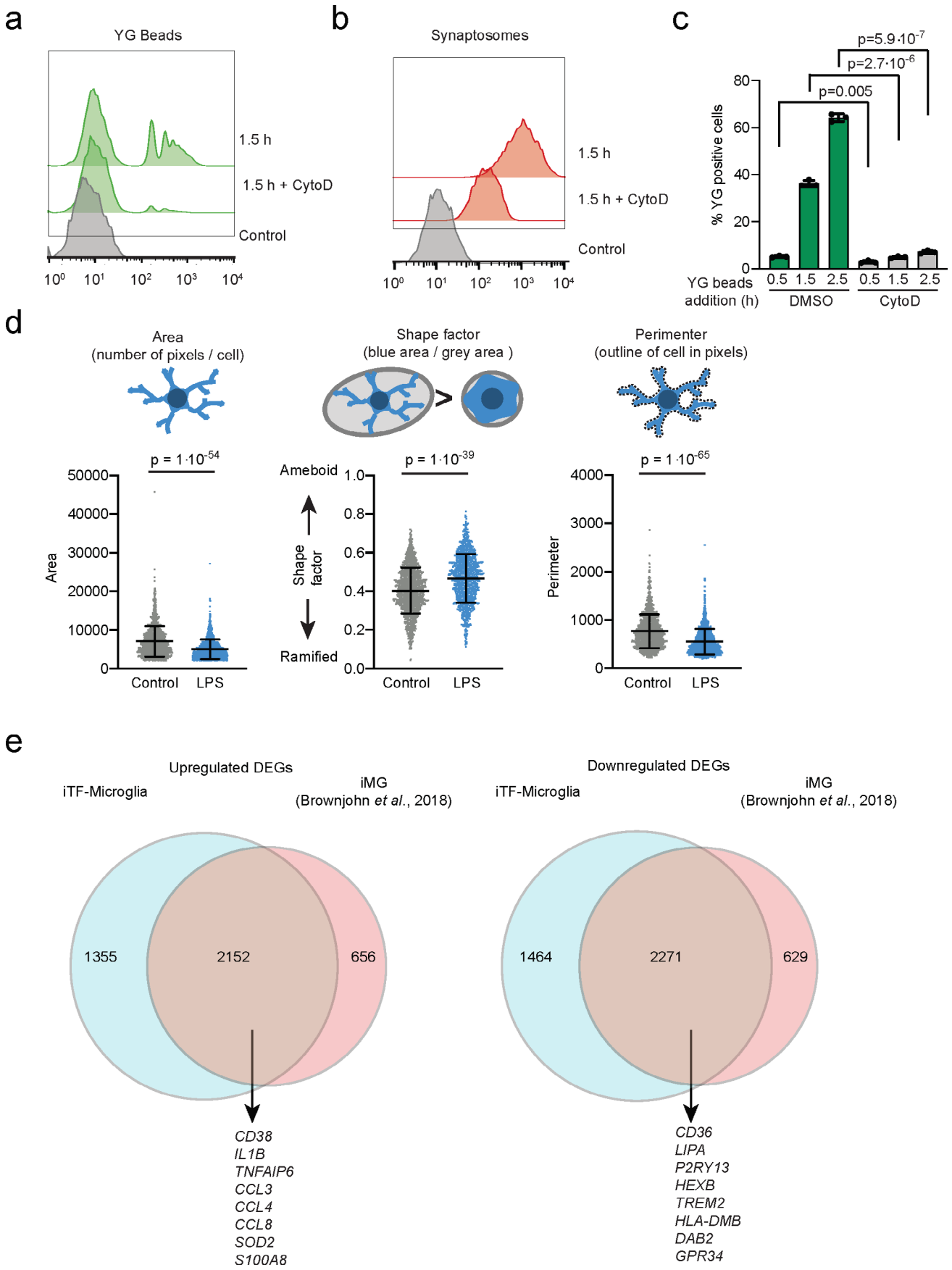


**Extended Data Fig. 2 | See next page for caption.**

**Extended Data Fig. 2 | Phagocytosis capacity of iTF-Microglia and morphological changes after LPS treatment. a**, **b**, Phagocytosis of yellow-green (YG) beads (a) or pHRodo-Red labeled synaptosomes (b) measured by flow cytometry. Histograms of YG-beads-FITC (a) and Synaptosome-PE (b) after 1.5 h of substrate exposure +/− 5 μM Cytochalasin D (CytoD) treatment. Controls are iTG-Microglia without substrate exposure. **c**, Phagocytosis of yellow-green (YG) beads at different timepoints. Flow cytometric quantification of the percentage of YG bead-positive cells at after 0.5 h, 1.5 h and 2.5 h of incubation with beads. Addition of 5 μM CytoD decreases the percentage of YG bead-positive cells. Means +/− sd, n = three individual biological replicates; p values from two-tailed Student's t-test. **d**, Morphological changes of iTF-Microglia after LPS treatment. Swarm plots showing the automated quantification of microglia F-actin staining in area, shape factor and perimeter with explanation of the three parameters. Means +/− sd, n = 16 wells from 3 individual differentiations; p values from two-tailed Mann-Whitney test. **e**, Comparison of differentially expressed genes in response to LPS treatment in iTF-Microglia versus iPSC-derived microglia (iMG) differentiated following a previously published protocol by Brownjohn *et al.*[18].

a

Karyotype: iTF-iPSC monoclonal line

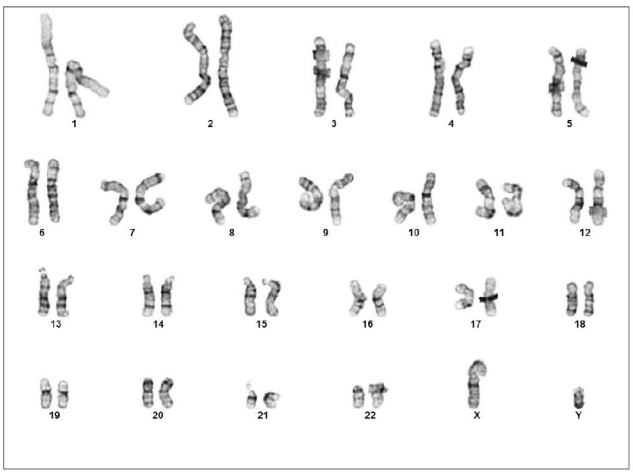

b

Karyotype: constitutive CRISPRi iTF-iPSC monoclonal line

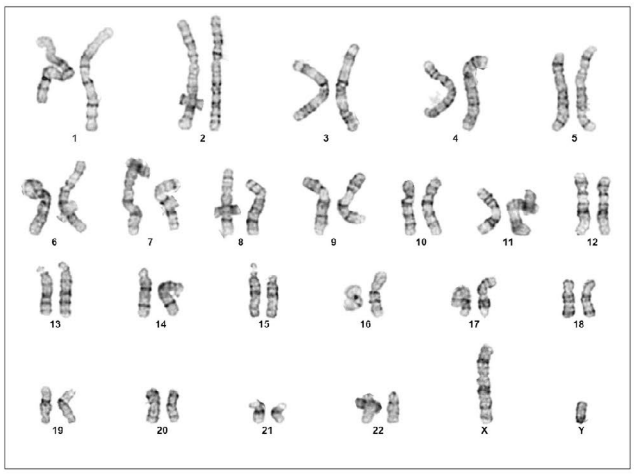

c

Karyotype: inducible CRISPRi iTF-iPSC monoclonal line

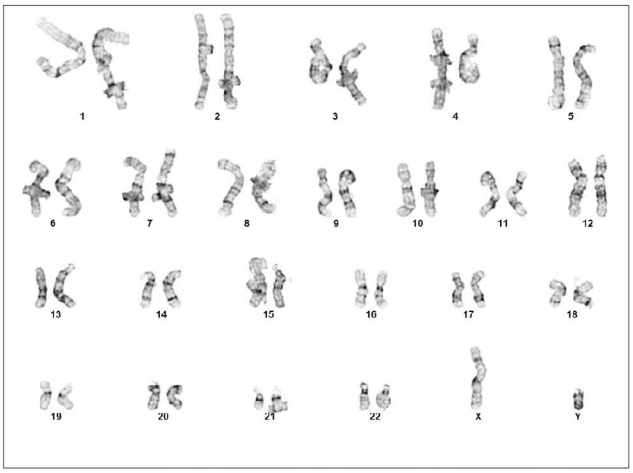

d

Karyotype: inducible CRISPRa iTF-iPSC monoclonal line

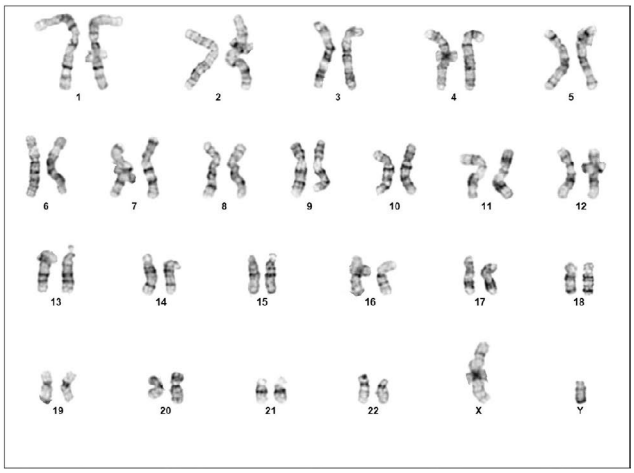

**Extended Data Fig. 3 | Karyotyping of the monoclonal iTF-iPSC lines.** A normal karyotype was confirmed for monoclonal lines **a**, iTF-iPSCs**, b**, constitutive CRISPRi iTF-iPSC, **c**, inducible CRISPRi iTF-iPSC, **d**, inducible CRISPRa iTF-iPSC lines.

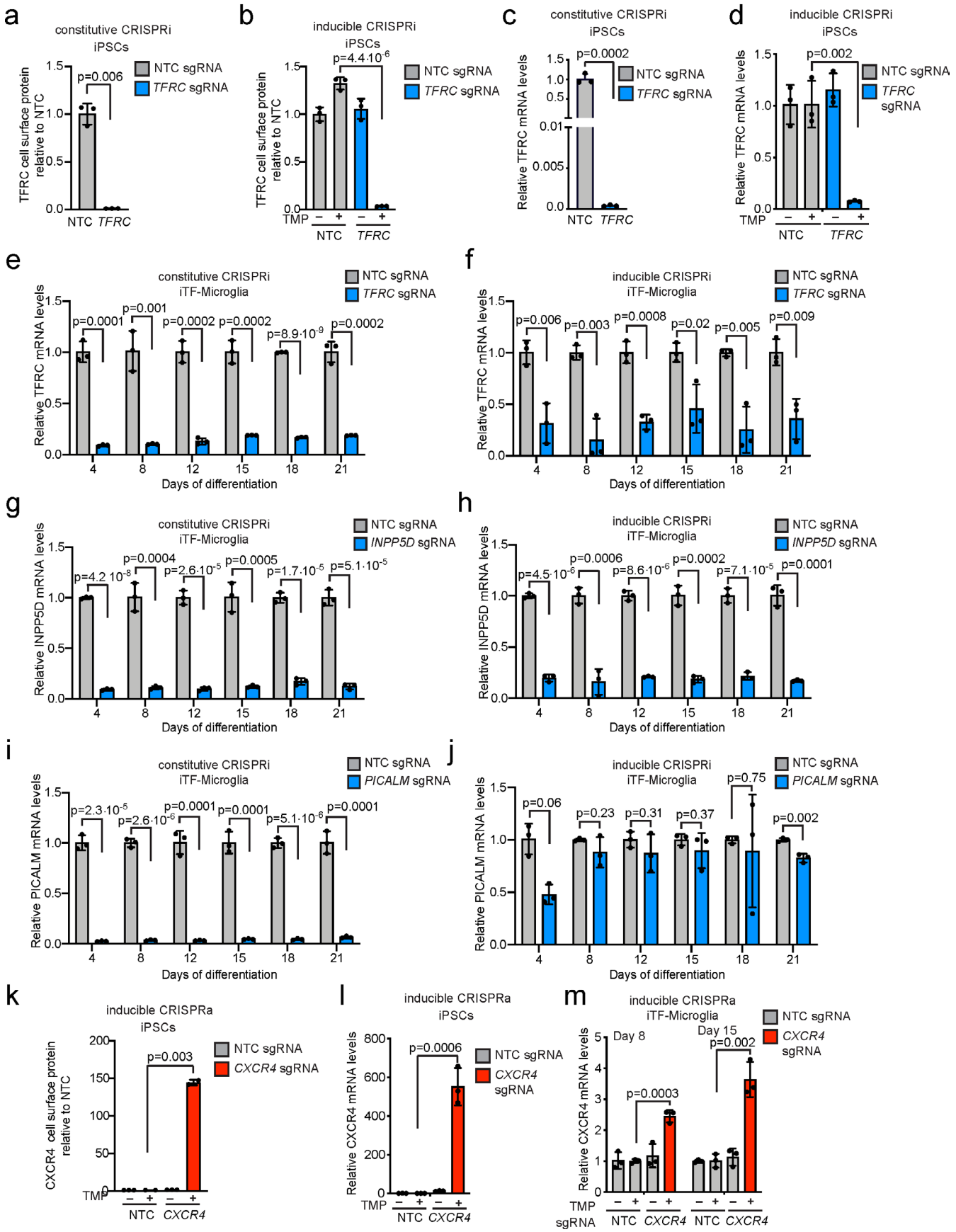


**Extended Data Fig. 4 | See next page for caption.**

**Extended Data Fig. 4 | Functional validation of CRISPRi/a activity in iPSCs and iTF-Microglia. a**, **b**, Functional validation of constitutive (a) or inducible (b) CRISPRi activity via flow cytometry of TFRC surface protein level stained iPSCs expressing a TFRC-targeting sgRNA or a non-targeting control (NTC) sgRNA (mean +/− sd, n = 3 biological replicates; p values from two-tailed Student's t-test). TMP was added to induce CRISPRi activity where indicated. **c-d, Knockdown of TFRC in iPSCs with (a) the constitutive and (b) the inducible CRISPRi system**. qPCR quantification of the relative fold change of TFRC mRNA levels in CRISPRi-iPSCs expressing a TFRC sgRNA as compared to a non-targeting control sgRNA in the presence or absence of trimethoprim (TMP). (mean +/− sd, n = 3 biological replicates; p values from two-tailed Student's t-test). TFRC levels were normalized to the housekeeping gene GAPDH. **e-j Knockdown of three different genes in iTF-Microglia with (e,g,i) constitutive CRISPRi and (f,h,j) inducible CRISPRi**. qPCR quantification of the relative fold change of *TFRC* mRNA levels (e,f), *INPP5D* mRNA levels (g,h) or *PICALM* mRNA levels (I,j) in CRISPRi-iTF-Microglia expressing a *TFRC* sgRNA (e,f), *INPP5D* sgRNA (g,h) or *PICALM* sgRNA (I,j) compared to a non- targeting control sgRNA at different days of differentiation in the presence of TMP (mean +/− sd, n = 3 biological replicates, P values from two-sided Student's t test). **k**, Functional validation of inducible CRISPRa activity via flow cytometry of CXCR4 surface protein level stained iPSCs expressing a CXCR4-targeting sgRNA or a non-targeting control (NTC) sgRNA (mean +/− sd, n = 3 biological replicates; p values from two-tailed Student's t-test). TMP was added to induce CRISPRi activity where indicated. **l-m**, qPCR quantification of the relative fold change of CXCR4 mRNA levels in inducible CRISPRa-iPSCs expressing a CXCR4 sgRNA as compared to a non-targeting control sgRNA in the presence or absence of trimethoprim (TMP), which stabilizes the DHFR degron. (mean +/− sd, n = 3 biological replicates; p values from two-tailed Student's t-test). CXCR4 levels were normalized to the housekeeping gene GAPDH.

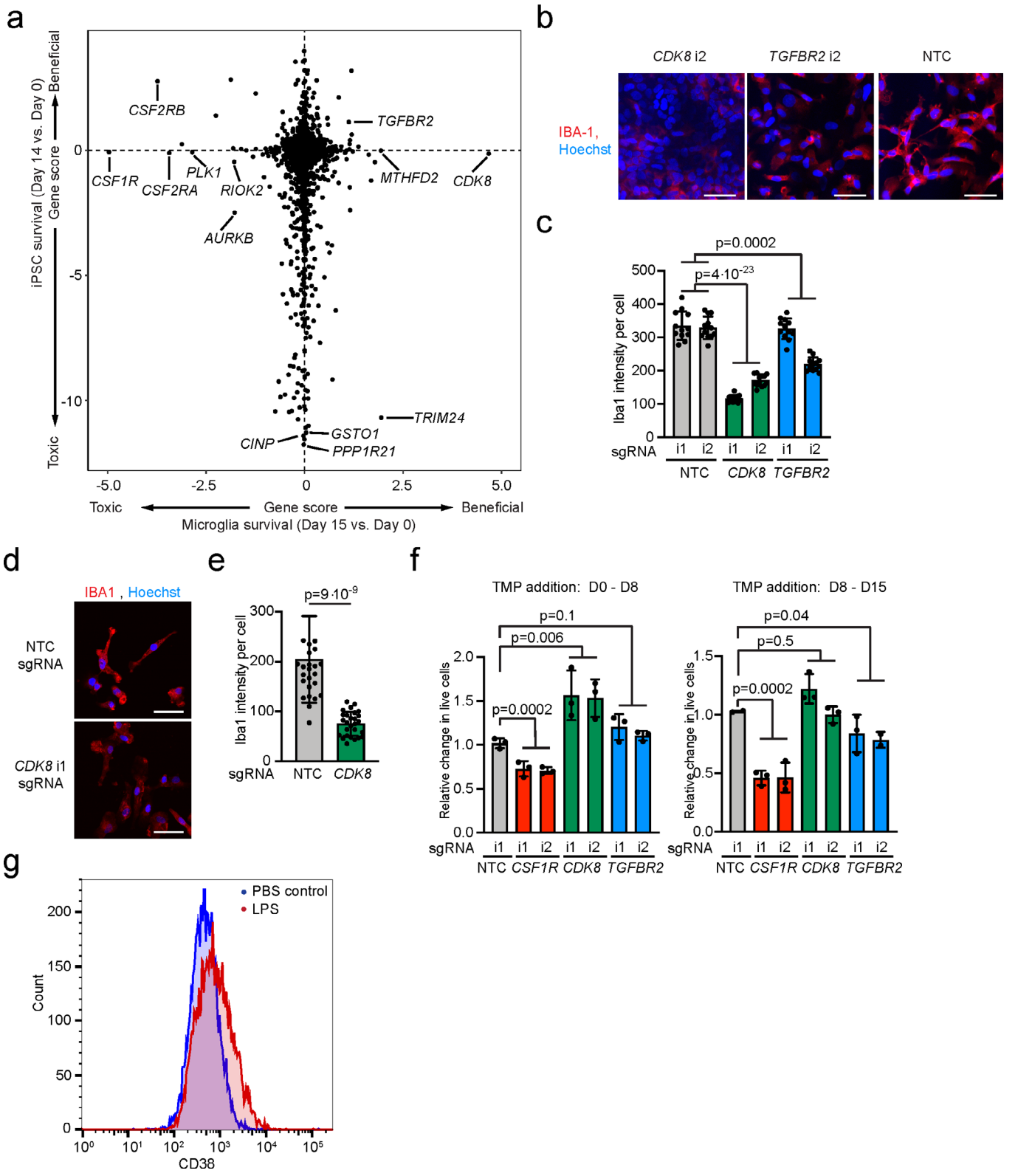


**Extended Data Fig. 5 | See next page for caption.**

**Extended Data Fig. 5 | Knockdown of *CDK8* and *TGFBR2* induces proliferation and decreases microglia markers in iPSC-derived microglia generated with different protocols. a**, Comparison of Gene Scores from CRISPRi survival/proliferation screens in iTF-Microglia (this study) vs. iPSCs[11]. Each dot represents a gene. **b-c**, IBA1 staining in Day 8 CRISPRi iTF-Microglia containing sgRNAs targeting *CDK8* or *TGFBR2* compared to non-targeting control (NTC) sgRNAs. **b**, Representative images. Scale bar = 50 μm. **c**, Quantification. Mean +/-sd, n = 6 fields of view from 2 different wells per sgRNA; p values from two-tailed Student's t-test. **d-e**, IBA1 staining in Day 8 iMGs generated by the protocol from Brownjohn *et al*., 2018 expressing sgRNAs targeting *CDK8* compared to non-targeting control (NTC) sgRNAs. **d**, Representative images. Scale bar = 50 μm. **e**, Quantification. Mean +/-sd, n = 9 fields of view from 3 different wells per sgRNA; p values from two-tailed Student's t-test. **f**, Relative change in live cells of iTF-Microglia at Day 8 (*left*) and Day 15 (*right*) containing sgRNAs targeting *CDK8*, *CSF1R* or *TGFBR2* compared to non-targeting control sgRNAs. The inducible CRISPRi system was stabilized with TMP from Day 0 – Day 8 (*left*) or Day 8 – Day 15 (*right*). (mean +/-sd, n = 3 biological replicates; p values from two-tailed Student's t-test. **g**, CD38 cell surface levels measured by flow cytometry in iTF-Microglia 24 h treatement with 100 ng/mL LPS or PBS control.

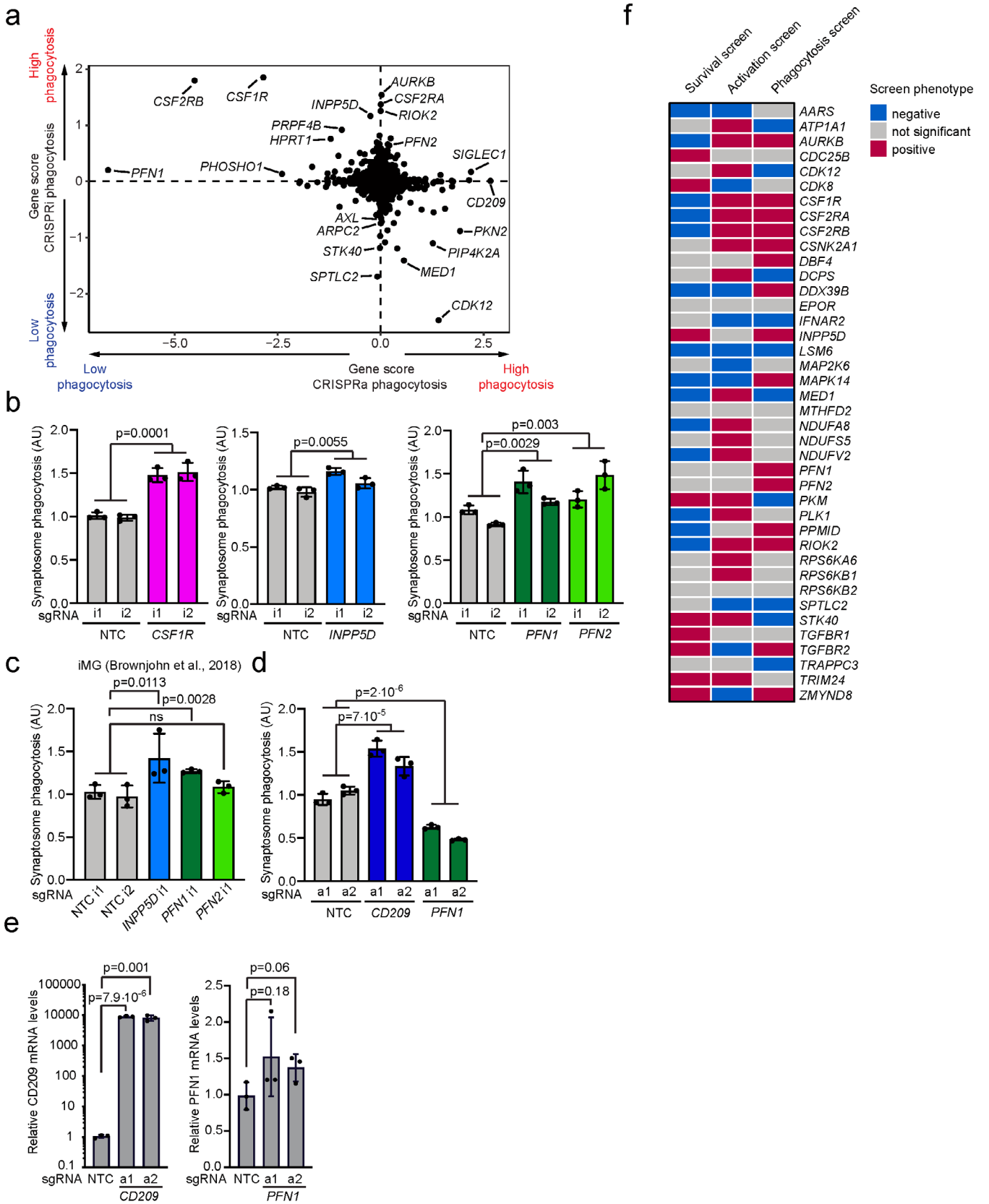


**Extended Data Fig. 6 | See next page for caption.**

**Extended Data Fig. 6 | Validation of phagocytosis hits and overview of genes selected for the CROP-seq screen based on primary screens. a**, Comparing Gene Scores for hits from phagocytosis CRISPRi and CRISPRa screens. Each dot represents a gene. **b-d**, Validation of (b,c) CRISPRi hits and (d) CRISPRa hits in (b,d) iTF-Microglia or (c) iPSC-derived microglia differentiated using an alternative protocol by Brownjohn *et al*.[18] Phagocytosis of pHrodo-labelled synaptosomes by cells expressing either non-targeting control (NTC) sgRNAs or sgRNAs targeting *CSF1R*, *INPP5D*, *PFN1* and *PFN2* was quantified by flow cytometry. Values represent mean +/− sd of n = 3 biological replicates; p values from two-tailed Student's t-test. **e**, Overexpression of CD209 (*left*) and PFN1 (*right*) with the inducible CRISPRa system in iTF-Microglia. QPCR quantification of the relative fold change of CD209 and PFN1 mRNA levels in iTF-Microglia expressing CD209 and PFN1 sgRNA as compared to a non-targeting control sgRNA in the presence of TMP (mean +/− sd, n = 3 biological replicates; p values from two-tailed Student's t-test). CD209 and PFN1 levels were normalized to the housekeeping gene GAPDH. **f**, Binary heatmap of genes selected for the CROP-seq screen and their knockdown phenotype in the CRISPRi survival, phagocytosis and inflammation screens. Red: KD increases phenotype (positive hit). Blue: KD decreases phenotype (negative hit). Grey: not a significant hit, $p > 0.1$.

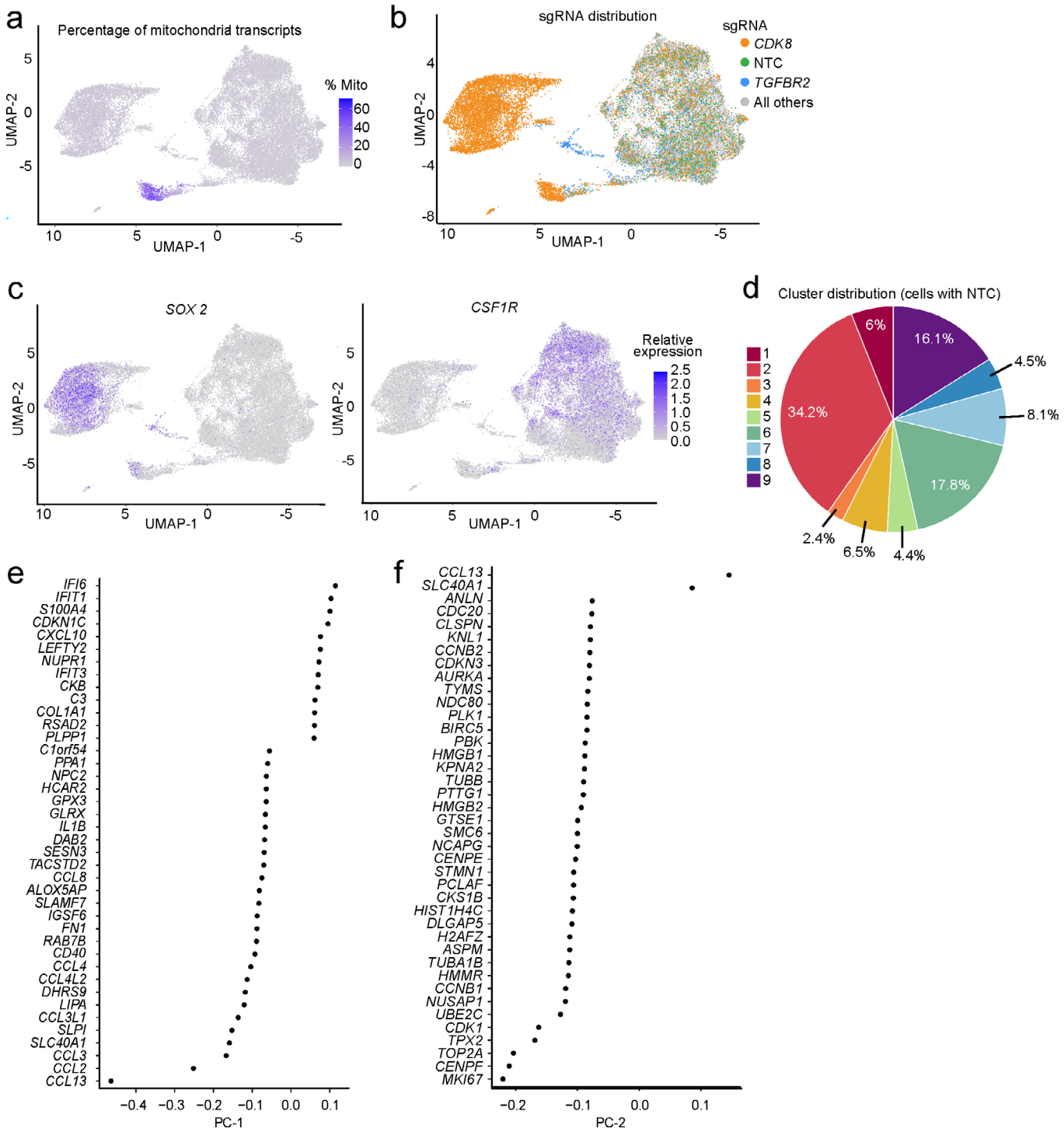


**Extended Data Fig. 7 | Characterization of microglia cluster signatures. a-c**, UMAP projection representing single-cell transcriptomes, with cells colored based on (a) the percentage of mitochondrial transcripts, (b) the expressed sgRNAs, with sgRNAs targeting *CDK8* in orange, sgRNAs targeting *TGFBR2* in blue, non-targeting control sgRNAs (NTC) in green, and all other sgRNAs in grey, or (c) expression levels of *SOX2* (*Left*) or *CSF1R* (*Right*). **d**, Distribution of iTF-Microglia expressing non-targeting (NTC) sgRNAs across the 9 clusters described in Fig. 6. **e**, **f**,the top 40 genes with the highest embedding values for (e) the first principal component (PC-1) and (f) the second principal component (PC-2), displayed in ranking order.

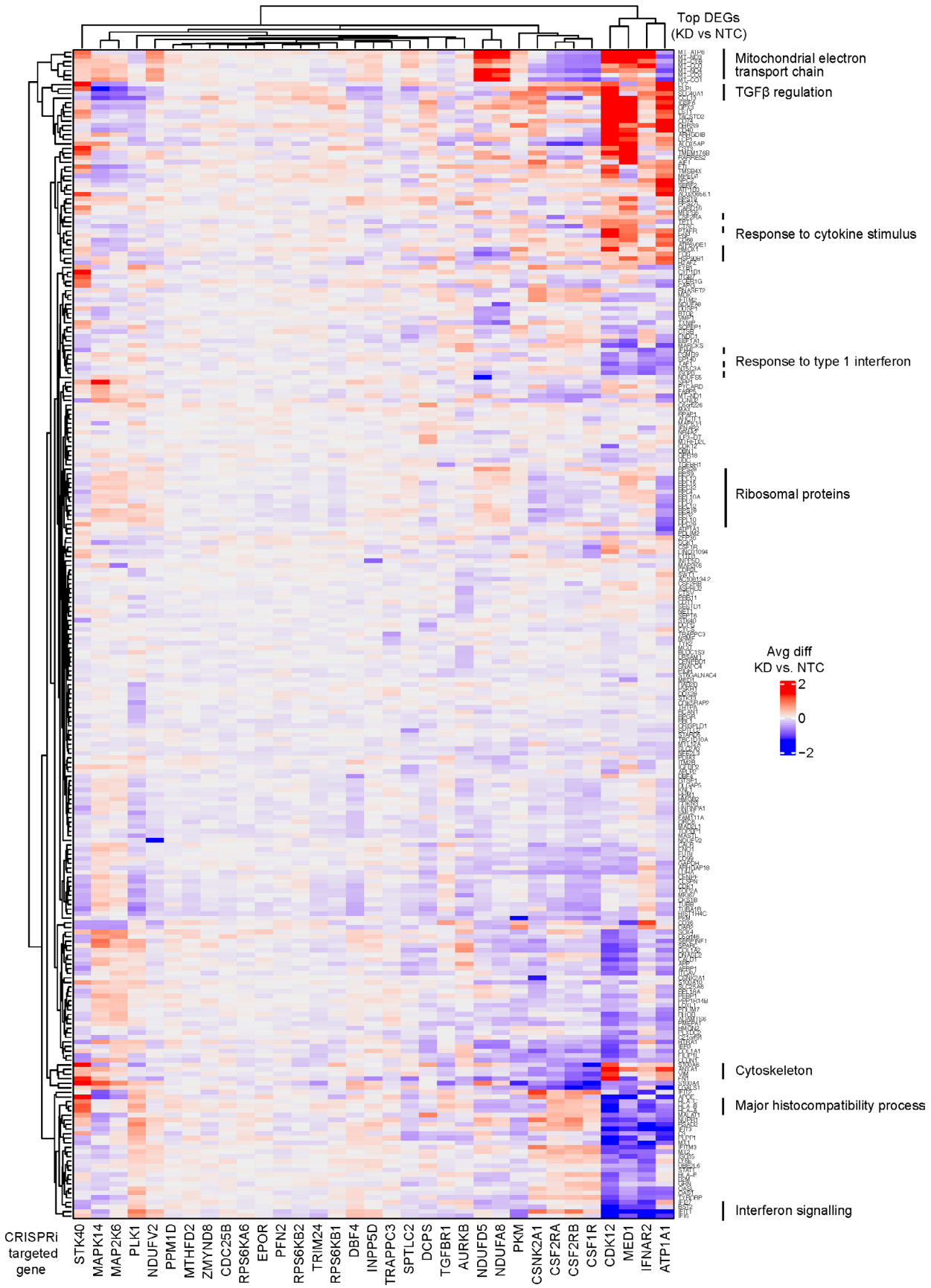


**Extended Data Fig. 8 | See next page for caption.**

**Extended Data Fig. 8 | CROP-seq reveals transcriptomic changes in iTF-Microglia induced by gene knockdown.** Changes in gene expression in response to CRISPRi knockdown of genes of interest in iTF-Microglia. Each column represents one CRISPRi-targeted gene. For each CRISPRi-targeted gene, cells with the strongest knockdown were selected and the top 20 differentially expressed genes in comparison to non-targeting control (NTC) sgRNA containing cells were selected. The merged set of these genes is represented by the rows. Rows and columns were clustered hierarchically based on Pearson correlation. Functionally related clusters of differentially expressed genes are labeled.

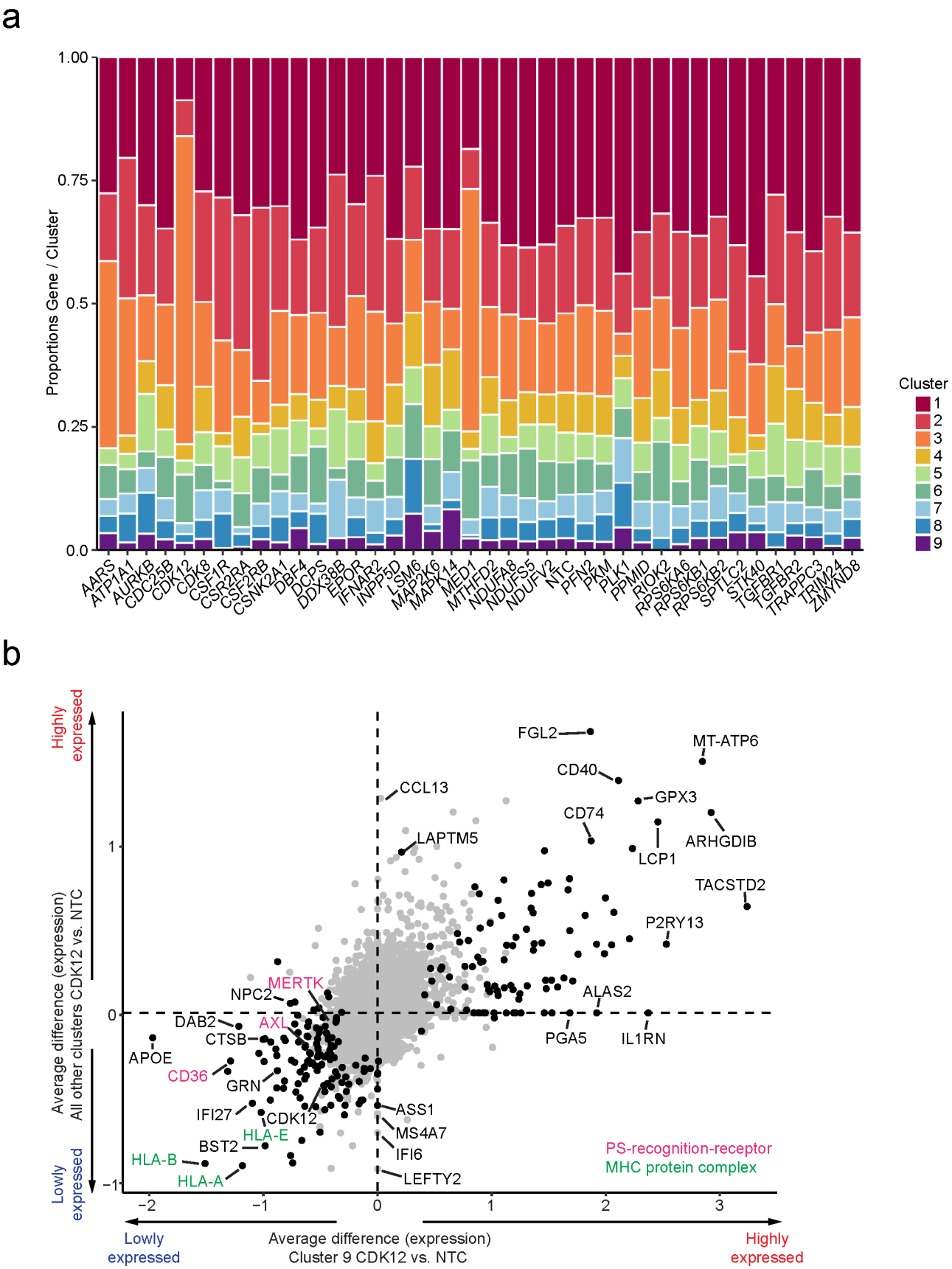


**Extended Data Fig. 9 | See next page for caption.**

**Extended Data Fig. 9 | Transcriptomic changes in iTF-Microglia induced by *CDK12* knockdown in cluster 9 and in all other clusters. a**, Changes in cluster distribution after CRISPRi knockdown of targeted genes in iTF-Microglia. Distribution of cells according to the 37 targeted genes and non-targeting control (NTC) in clusters 1–9. **b**, Average differences of gene expression induced by *CDK12* knockdown in cluster 9 compared to those in all other clusters. Genes encoding phosphatidylserine (PS) recognition receptors are labeled in magenta and Genes encoding MHC complex components are labeled in green.

nature research

Corresponding author(s): Martin Kampmann, Li Gan

Last updated by author(s): Jun 23, 2022

# Reporting Summary

Nature Research wishes to improve the reproducibility of the work that we publish. This form provides structure for consistency and transparency in reporting. For further information on Nature Research policies, see Authors & Referees and the Editorial Policy Checklist.

## Statistics

For all statistical analyses, confirm that the following items are present in the figure legend, table legend, main text, or Methods section.

| n/a | Confirmed | |
|---|---|---|
| ☐ | ☒ | The exact sample size (*n*) for each experimental group/condition, given as a discrete number and unit of measurement |
| ☐ | ☒ | A statement on whether measurements were taken from distinct samples or whether the same sample was measured repeatedly |
| ☐ | ☒ | The statistical test(s) used AND whether they are one- or two-sided<br>*Only common tests should be described solely by name; describe more complex techniques in the Methods section.* |
| ☒ | ☐ | A description of all covariates tested |
| ☐ | ☒ | A description of any assumptions or corrections, such as tests of normality and adjustment for multiple comparisons |
| ☐ | ☒ | A full description of the statistical parameters including central tendency (e.g. means) or other basic estimates (e.g. regression coefficient) AND variation (e.g. standard deviation) or associated estimates of uncertainty (e.g. confidence intervals) |
| ☐ | ☒ | For null hypothesis testing, the test statistic (e.g. *F*, *t*, *r*) with confidence intervals, effect sizes, degrees of freedom and *P* value noted<br>*Give P values as exact values whenever suitable.* |
| ☒ | ☐ | For Bayesian analysis, information on the choice of priors and Markov chain Monte Carlo settings |
| ☒ | ☐ | For hierarchical and complex designs, identification of the appropriate level for tests and full reporting of outcomes |
| ☐ | ☒ | Estimates of effect sizes (e.g. Cohen's *d*, Pearson's *r*), indicating how they were calculated |

*Our web collection on statistics for biologists contains articles on many of the points above.*

## Software and code

Policy information about availability of computer code

| | |
|---|---|
| Data collection | For FACS data collection, we used BD FACSDiva (version 8.0.1.1). For microscopy data collection by InCell 6000, we used In Cell Analyzer 6000 Acquisition Software (version 4.0). For qPCR data collection, we used Quant Studio Real Time PCR software (version 1.3). For cytokine array imaging, we used Image Studio (version 5.2). For Cell-TiterGlo luminescence data collection, we used SoftMax Pro 6.5.1. |
| Data analysis | For FACS analysis, we used FlowJo (version 10.7.1) and Prism 8 (8.4.2). For microscopy image analysis we used Fiji (version 2.0.0) and CellProfiler (version 4.1.3). For pooled CRISPR screen analysis, we used MAGeck-iNC (version 5.2) and Bowtie (version 0.12.9). For bulk RNA-seq analysis, we used Salmon (version 1.4.0), Tximport (version 1.18.0), ggplot2 (version 3.3.3), Complex Heatmap (version 2.6.2), DESeq2 (version 1.30.1), and VennDiagram (version 1.6.20). For CROP-seq analysis, we used Cell Ranger (version 5.0.1), in R (version 4.0.3) we used DropletUtils (version 1.10.3) and Seurat (4.0.1).<br>The MAGeCK-iNC bioinformatics pipeline for analysis of pooled screens available at https://kampmannlab.ucsf.edu/mageck-inc. The R notebooks for the RNA-seq and CROP-seq analysis are available at https://kampmannlab.ucsf.edu/article/microglia-analysis. The CellProfiler pipelines will be made available on request to the corresponding authors (MK), and will also be submitted to the CellProfiler depository of published pipelines (https://cellprofiler.org/examples/published_pipelines.html) upon publication. |

For manuscripts utilizing custom algorithms or software that are central to the research but not yet described in published literature, software must be made available to editors/reviewers. We strongly encourage code deposition in a community repository (e.g. GitHub). See the Nature Research guidelines for submitting code & software for further information.

## Data

Policy information about availability of data

All manuscripts must include a data availability statement. This statement should provide the following information, where applicable:

- Accession codes, unique identifiers, or web links for publicly available datasets
- A list of figures that have associated raw data
- A description of any restrictions on data availability

All screen datasets and RNA-transcriptomic datasets are publicly available in the CRISPRbrain data commons (http://crisprbrain.org/) (associated with Figures 1, 2, 4,

5, 6, 7 and Extended Data Figures 1, 4, 5, 6, 7). RNA sequencing datasets reported in this paper are available on NCBI GEO, accession number GSE178317 (https://www.ncbi.nlm.nih.gov/geo/query/acc.cgi?acc=GSE178317). There are no restrictions on data availability.

# Field-specific reporting

Please select the one below that is the best fit for your research. If you are not sure, read the appropriate sections before making your selection.

☒ Life sciences ☐ Behavioural & social sciences ☐ Ecological, evolutionary & environmental sciences

For a reference copy of the document with all sections, see nature.com/documents/nr-reporting-summary-flat.pdf

# Life sciences study design

All studies must disclose on these points even when the disclosure is negative.

| | |
|---|---|
| Sample size | Sample sizes were determined by existing studies in the field to enable statistical analyses and reproducibility, specifically our previous CRISPRi screens in iPSC-derived neurons (Tian et al. 2019, Neuron 104:239-255). |
| Data exclusions | No data was excluded from the relevant analyses. |
| Replication | Major findings were validated using independent samples and orthogonal approaches. Numbers of replicates are listed in each Figure. |
| Randomization | No randomization of samples was used since treatment group of cells were generally derived from the same population of cells. |
| Blinding | Blinding was not relevant to our study since no subjective rating of data was involved. Instead, we used computational quantification. |

# Reporting for specific materials, systems and methods

We require information from authors about some types of materials, experimental systems and methods used in many studies. Here, indicate whether each material, system or method listed is relevant to your study. If you are not sure if a list item applies to your research, read the appropriate section before selecting a response.

## Materials & experimental systems

| n/a | Involved in the study |
|---|---|
| ☐ | ☒ Antibodies |
| ☐ | ☒ Eukaryotic cell lines |
| ☒ | ☐ Palaeontology |
| ☒ | ☐ Animals and other organisms |
| ☒ | ☐ Human research participants |
| ☒ | ☐ Clinical data |

## Methods

| n/a | Involved in the study |
|---|---|
| ☒ | ☐ ChIP-seq |
| ☐ | ☒ Flow cytometry |
| ☒ | ☐ MRI-based neuroimaging |

## Antibodies

| | |
|---|---|
| Antibodies used | Primary antibodies: IBA-1 (1:1000, Wako; Cat. No. 019-19741), GPR34 (1:150, R&D Systems; Cat. No. MAB4617), TFRC (1:200, abcam ; Cat. No. ab84036), Synaptophysin (1:1000, Synaptic Systems; Cat. No. 101004).<br><br>Secondary antibodies: Alexa Fluor 488 goat anti rabbit IgG (1:500, Invitrogen; Cat. No. A11034), Alexa Fluor 488 goat anti mouse IgG (1:500, Invitrogen; Cat. No. A11029), Alexa Fluor 568 goat anti rabbit IgG (1:500, Invitrogen; Cat. No. A11036), Alexa Fluor 647 goat anti-chicken IgG (1:500 dilution; abcam Cat. No. ab 150171)<br><br>Coupled antibodies: PE-Cy7 anti-human CD71 (TFRC) (1: 66, BioLegend; Cat. No. 334112), PE/Cy7 anti-human CD184 (CXCR4) (1:66, BioLegend; Cat. No. 306514), Human CCL13 488 (1:75, R&D Systems; Cat. No. IC327G), hCD38 PE (1:200, R&D Systems; Cat. No. FAB2404P), hOsteopontin eFluor 660 (1:75, eBioscience ; Cat. No. 50-9096-42). |
| Validation | Antibodies were validated by the manufacturers as follows: Anti-IBA-1 (Wako; Cat. No. 019-19741) was validated by immunohistochemistry of microglia in rat cerebral cortex and mouse cerebellum. Anti-GPR34 (R&D Systems; Cat. No. MAB4617) has been validated by staining human GPR34 transfectants but not irrelevant transfectants. Anti-Synaptophysin (Synaptic Systems; Cat. No. 101004) was validated by western blotting of a synaptosomal fraction of rat brains and validated by immunostaining of hippocampal neurons. Anti-TFRC (abcam ; Cat. No. ab84036) was validated by western blotting of various cell lysates, detecting a clear band of approximately 98 kDa (predicted molecular weight: 84 kDa). |

## Eukaryotic cell lines

Policy information about cell lines

| | |
|---|---|
| Cell line source(s) | The human iPSC line WTc11 was obtained from Coriell (GM25256). The human iPSC line WTc11 was obtained with CRISPRi machinery was obtained from Coriell (AICS-0090-391). HEK293T cells were obtained from ATCC (CRL-3216). |
| Authentication | iPSCs were karyotyped (Extended Data Fig. 3) and characterized for maintaining capability to differentiate into iTF-Microglia. AICS-0090 cl.391 was authenticated by the Allen Institute for Cell Science. We did not authenticate the HEK293T cells. |
| Mycoplasma contamination | All lines were tested negative for mycoplasma using the Universal Mycoplasma Detection Kit (ATCC 30-1012KTM). |
| Commonly misidentified lines (See ICLAC register) | No commonly misidentified lines were used. |

## Flow Cytometry

### Plots

Confirm that:

☒ The axis labels state the marker and fluorochrome used (e.g. CD4-FITC).

☒ The axis scales are clearly visible. Include numbers along axes only for bottom left plot of group (a 'group' is an analysis of identical markers).

☒ All plots are contour plots with outliers or pseudocolor plots.

☒ A numerical value for number of cells or percentage (with statistics) is provided.

### Methodology

| | |
|---|---|
| Sample preparation | Cells were dissociated using Accutase (for iPSCs) or TrypIE (for iTF-Microglia) and analyzed or sorted by flow cytometry based on staining signals. For cell surface receptor stainings, dissociated and in DPBS resuspended iTF-Microglia were blocked for 15 min with 1:20 Human FC Block (BD Biosciences; Cat. No. 564220). For CRISPRi/a validation, cells were stained with 1:66 PE/Cy7 anti-human CD184 (CXCR4) (BioLegend; Cat. No. 306514) or 1:66 PE-Cy7 anti-human CD71 (TFRC) (BioLegend; Cat. No. 334112) for 30 min in the dark. Cells were washed twice with DPBS before analyzing them by flow cytometry. For the CD38 screen and validation experiments, iTF-Microglia were stained with 1:200 anti-hCD38 PE (R&D Systems; Cat. No. FAB2404P). Cells were washed twice with DPBS before analyzing them by flow cytometry.<br>For intracellular protein staining, dissociated iTF-Microglia were fixed and permeabilized with the eBioscience Intracellular Fixation and Permeabilization Buffer Set (Invitrogen; Cat. No. 88-8824-00) according to the manufacturer's instructions. Cells were stained with 1:75 Anti-Hu Osteopontin (SPP1) eFluor 660 (eBioscience; Cat. No. 50-9096-42) or 1:75 Human CCL13 488 (R&D Systems; Cat. No. IC327G) or their isotype controls Mouse IgG1 Control Alexa Fluor 488 conjugated (R&D Systems; Cat. No. IC002G) and Mouse IGG1 kappa Isotype (eBioscience; Cat. No. 50-4714-82) over night at 4°C. Cells were washed twice with DPBS before analyzing them by flow cytometry. For analyzing phagocytosis rates and the phagocytosis screen, cells were washed twice with DPBS, dissociated, resuspended in ice-cold DPBS, and then analyzed via flow cytometry. |
| Instrument | BD LSRFortessa X14 and BD FACSAria Fusion |
| Software | BD FACSDiva (version 8.0.1.1) and FlowJo (version 10.4) |
| Cell population abundance | To analyze staining signals or uptake of fluorescent materials (beads or synaptosomes), cells were analyzed and not sorted. The starting populations were pure (either iPSCs or iTF-Microglia). For pooled screens, iTF-Microglia were sorted into high and low signal populations corresponding to the top 30% and the bottom 30% of the staining signal distribution. |
| Gating strategy | Preliminary FSC/SSC gates encompassed all live, single cells in the population. For pooled screens, these cells were sorted into high and low signal populations corresponding to the top 30% and the bottom 30% of the staining signal distribution. |

☒ Tick this box to confirm that a figure exemplifying the gating strategy is provided in the Supplementary Information.